2013

Polymeric Radiation Shielding for Applications in Space: Polyimide Synthesis and Modeling of Multi-Layered Polymeric Shields

Clinton Cleveland Schiavone
College of William & Mary - Arts & Sciences

Polymeric Radiation Shielding for Applications in Space: Polyimide Synthesis and Modeling of Multi-layered Polymeric Shields

Clinton Cleveland Schiavone

Winchester, Virginia

B.S. of Chemistry, the College of William and Mary, 2011

A Thesis presented to the Graduate Faculty
of the College of William and Mary in Candidacy for the Degree of
Master of Science

Department of Chemistry

The College of William and Mary
January, 2013

APPROVAL PAGE

This Thesis is submitted in partial fulfillment
of
the requirements for the degree of

Master of Science

Clinton Cleveland Schiavone

Approved by the Committee, December, 2012

Committee Chair
Professor Emeritus Dr. Robert A. Orwoll, Chemistry
College of William and Mary

Professor Emeritus Dr. Richard L. Kiefer, Chemistry
College of William and Mary

Floyd Dewey Gottwald, Sr. Professor Dr. Robert D. Pike, Chemistry
College of William and Mary

Professor Dr. Gary W. Rice, Chemistry
College of William and Mary

ABSTRACT

Exposure to high-energy Galactic Cosmic Radiation (GCR) is one of the major barriers in the advancement of manned space missions. GCR is incident from outside the solar system and among the highest energy events observed by man. The Earth's surface is protected by its geomagnetic fields that trap incoming charged radiation in the Van Allen Belts. NASA has cited these different forms of radiation as key problems to overcome for interplanetary space travel to become a reality.

This work intends to address the development of adequate radiation shielding for space applications from two different directions. The first method is the chemical synthesis and modification of polyimides as well as doping with additives for specific absorptions of targeted components and products of GCR. The second approach is to model and simulate polymeric shielding systems subject to GCR heavily utilizing NASA's OLTARIS program. Of particular interest are the effects within multi-layered systems.

Layered systems of materials were studied to identify key relationships and effects present. Every test has shown that any layer in a system has an influence on the shielding performances of the other layers both before and after it. It was found that placing polypropylene in a layer at the backside of a shield greatly enhances the shielding. Large concentrations of metals have little effect on shielding if there is a polypropylene layer behind it. This work proposes and evaluates a multi-layered shield composed of polypropylene and doped polyimides. Other modeling trials compare the shielding capabilities of polymers in low Earth orbit (LEO) and free space environments.

TABLE OF CONTENTS

ACKNOWLEDGEMENTS

I wish to express my gratitude to my mentor, Dr. Robert Orwoll, under whose direction this work was conducted, for his inspiration in learning and teaching. I am also indebted to Dr. Kiefer for his all help in my work.

This work was also made possible through the generous aid of Dr. Eugene Aquino and Dr. Russel Churchill of International Scientific Technologies, Inc.

I would also like to gratefully recognize NASA for their funding of the research that is presented herein. Funding came through SBIR/STTR grants, NNX11CI31P and NNX11CB81C, awarded to the collaboration of International Scientific Technologies, Inc. and the College of William and Mary.

This Masters is dedicated to my family, who have always nurtured and supported my love and perpetual study of nature.

PROBLEM

The advancement of human space exploration via manned spacecraft beyond the region protected by the earth's magnetic field cannot proceed until high-energy space radiation and its effects are better understood. Some of these environmental hazards in space are the highest energy events observed by man. Adequate shielding of this incident space radiation must be achieved if we are to probe deeper in our endeavor to better comprehend the universe and progress our physical manifestation beyond the earth and its moon.

RESEARCH BACKGROUND

Earth's magnetic fields protect us residing on and near its surface from incoming charged-particle radiation. The charged matter is effectively captured and retained in two "belts" that are known as the Van Allen Belts. These belts range in distance above the earth, starting at 10,000 km and extending all the way to 60,000 km away. The only time man ventured outside of these fields and into the free space environment was in NASA's Apollo missions. The charged particles collected from incoming radiation and concentrated at the poles by the earth's magnetic fields can be seen on earth's surface in the Aurora Borealis and Aurora Australis phenomena. Past these belts and the Earth's geomagnetic sphere the space environment become much more precarious.

Galactic Cosmic Radiation (GCR) is the form of space radiation that presents the greatest environmental hazard. The radiation comes from outside of our solar system and contains such high energy, as much as several hundred GeV, it can only be hypothesized what events in our universe could be the source. The radiation is comprised of the bare nuclei of all elements, though mostly nuclei of hydrogen (85%) and helium (14%)[1]. While nuclei of all elements are observed in GCR, the elemental distribution beyond hydrogen and helium strongly peaks with iron nuclei. This radiation can penetrate the hull of a space craft (an aluminum shell in most cases) and sometimes causes nuclear fragmentation with the nuclei present in the vessel walls. This nuclear fragmentation produces secondary radiation consisting mostly of free neutrons, smaller nuclei and electromagnetic radiation in the form of gamma-rays and

X-rays. The energy of the incident GCR nuclei is mostly dampened through Coulombic interactions with the shielding material.

A large portion of the **secondary radiation** products from nuclear collisions of incident nuclei and the target nuclei continues onward through the shielding material. Even though this radiation is not as high energy as the incident it still poses significant hazard to the vessel in space and its inhabitants. Research has shown that while the actual number of collisions between heavy ions and the shield are only a small fraction of the total interactions, they very well may be responsible for a substantial portion of the effective dose of radiation while in space[2]. The electromagnetic portions, gamma- and X-rays, are observed and have synthetic sources on earth. Large nuclei perform best at absorbing these high-energy, low-wavelength emissions with many terrestrial applications being the extremely effective use of lead and leaded glass in absorbing X-rays. The other part of secondary radiation that warrants optimized shielding is the neutrons created and emitted in nuclear fragmentation events. Neutrons behave differently than gamma rays and X-rays. They do not directly cause ionization, but through capture can create unstable isotopes that can undergo particle decay, releasing harmful radiation. Nuclei highly susceptible to neutron absorption are sought to be incorporated into the shielding systems to prevent hazardous levels of free neutrons ejecting out the backside.

Solar Particle Events (SPE) are another form of high-energy radiation that is found in space. This radiation is emitted from the sun at our solar system's gravitational center in events such as coronal mass ejections and solar flares and is made up almost completely of protons, but heavier nuclei (mostly helium) are also

observed at much lower levels. The levels of radiation observed from SPE and GCR are inversely related. The maximum in GCR was observed in 1977 when SPE experienced a minimum. This can be attributed to the strong electro-magnetic field carried with SPE that disrupts incoming GCR encountered in the path as the SPE radiates outward, projected from the sun[3]. While very sudden, violent and high-energy events, particles from SEP "storms" are still not nearly as high energy as incoming GCRs, but they are intense enough to deliver lethal doses[4]. It is assumed that a good shield for GCR would also be highly effective shielding for SEP.

The best practical shielding of GCR is currently obtained through two polymers with identical empirical formulas of CH_2, polyethylene and polypropylene. Their effectiveness stems from their high hydrogen content. Hydrogen, being neutron free, has the greatest charge-to-mass ratio of any element and thus creates the highest degree of Coulombic interactions with the incident high energy nuclei. Hydrogen also cannot be fragmented in collisions with the GCR.

Additives are incorporated into polymers, seeking to improve and impart beneficial properties to the shields. The additives in this work can be obtained in a foil or in powder-like nanoparticles. If a salt or nanopowder incorporation approach is taken, the additives must be well dispersed to create an ideal, homogenous shield. Gadolinium, boron, and tungsten are three candidate additives for enhanced capture of secondary radiation.

Gadolinium is a rare-earth metal with atomic number 64 and a melting point of 1312°C. Even though it has a relatively low density for a metal, 7.9 g/cm^3, gadolinium-157 has been identified as possessing the largest cross-section for the

absorption of thermal neutrons of any stable isotope. This makes it a premier additive for neutron absorption applications requiring no costly isotopic enrichment. The other five stable isotopes of gadolinium, with masses from 154-160 amu, are also capable of significant neutron absorption. Its large atomic number also makes it a suitable candidate for absorption of electromagnetic secondary radiation.

Boron, of atomic number 5 and with a density of 2.4 g/cm^3, is the smallest element believed to be a suitable additive to materials in the studies outlined herein. Boron's melting temperature is fairly high at 2076°C. Boron-11 is the most abundant isotope but boron-10 has a high probability for neutron absorption. In fact it has the largest thermal neutron capture cross-section per unit mass of any element. In space applications, minimizing weight is always a critical aspect of feasibility analysis.

Tungsten is a transition metal, atomic number 74, and has the second highest melting point (over 3400°C) of any element. It has a large density, 19.25 g/cm^3, almost that of gold. Because of its high atomic number it is an attractive option for absorbing high energy electromagnetic radiation. Its stout physical characteristics also may be beneficial in improving the physical capabilities (i.e. tensile strength, load bearing capacity, etc.) of the material doped.

Silver, atomic number 47, has the highest electrical conductivity of any element. Using silver as an additive, electrical charges imparted from GCR could possibly be mitigated away from sensitive electrical components.

PROPOSED SOLUTION

A material is required that adequately shields the intensive and harmful radiation present in the space environment. Minimizing the weight of the shielding materials and reducing maintenance requirements are necessities in determining the feasibility of a shield. The ideal shield should also be physically durable and thermally stable to withstand the harsh conditions of space. Some polymers fit all these requirements.

Polymers are lightweight materials that can be modified in chemical structure and used in composites for specific applications. Polymers also have potential as structural components in space applications as well as radiation shielding. As mentioned, the high-hydrogen content polymers, polypropylene and polyethylene, are the most effective known polymer shields for GCR. Due to their aliphatic nature, these polymers have poor thermal and mechanical properties when compared to other polymers such as polyimides. Table 1 compares some basic physical and mechanical properties of polyethylene, polypropylene, and the polyimides Kapton and Ultem 1000.

Polymer	Minimum Service Temperature (°C)	Maximum Service Temperature (°C)	Tensile Strength (psi)
High Density Polyethylene	-100	120	4550
Polypropylene	0	135	4500
Kapton Polyimide	-269	400	33500
Ultem 1000	-----	171	16500

Table 1: Thermal and mechanical properties of high density polyethylene[5], polypropylene[6], Kapton[7], and Ultem 1000[8].

Polyimides, specifically Kapton and Ultem 1000, have been utilized in NASA missions, mostly as insulation for the spacecraft and electronics because of their wide range of thermal stability. The aromatic structure of polyimides also significantly enhances their mechanical properties due to the high rigidity of the rings.

This research has taken a two-pronged approach to meeting the needs of polymeric radiation shielding for space applications: synthesis and modification of polyimides, as well as modeling and analyzing polymeric materials for shielding effectiveness. Multiple polyimides have been created, as well as the synthesis of a diamine monomer. A doped polyimide system has been synthesized for electronic applications in space. Modeling and analyses of polymer radiation shields was conducted with the use of OLTARIS, the On-Line Tool for the Assessment of Radiation In Space, a website-based program provided by NASA. The results of modeling were then used to propose a multi-layered polymeric radiation shield.

SYNTHESIS

Polyimides have been identified as ideal candidate polymers for this works' desired space applications. This work in synthetic polymer chemistry describes a polyimidization procedure, the modification of a polyimide through the incorporation of silver as a complex, and the synthesis of a diamine monomer.

Polyimide Synthesis

The repeating monomer units that make up polyimide chains can be tailored to fit specific needs by deliberate selection of the monomer cores. The synthetic pathways are maintained even when these monomer cores are varied. Table 2 shows the structure of four polyimide monomers, two diamines and two dianhydrides.

Polyimide Monomers	
Diamines	**Dianhydrides**
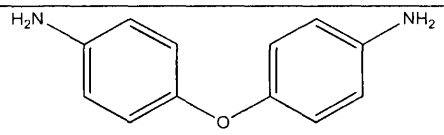 4,4'-Oxydianiline (ODA)	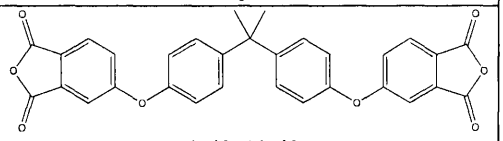 4,4'-(4,4'-Isopropylidenediphenoxy)bis(phthalic anhydride) (UDA- Ultem Dianhydride)
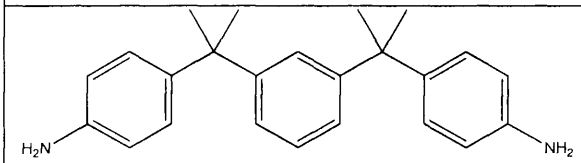 4,4'-(1,3- Phenylenediisopropylidene) bisaniline (BAM)	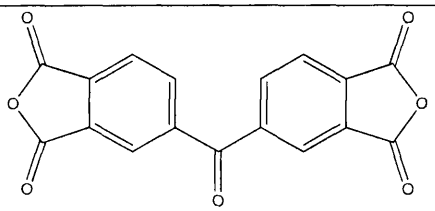 Benzophenone-3,3',4,4'-tetracarboxylic dianhydride (BTDA)

Table 2: Polyimide Monomers.

In the synthesis of a polyimide, it is necessary to react equimolar amounts of a diamine and a dianhydride to facilitate the formation of a long chain molecule comprised of a single repeating unit. An example polyimidization is illustrated in Figure 1.

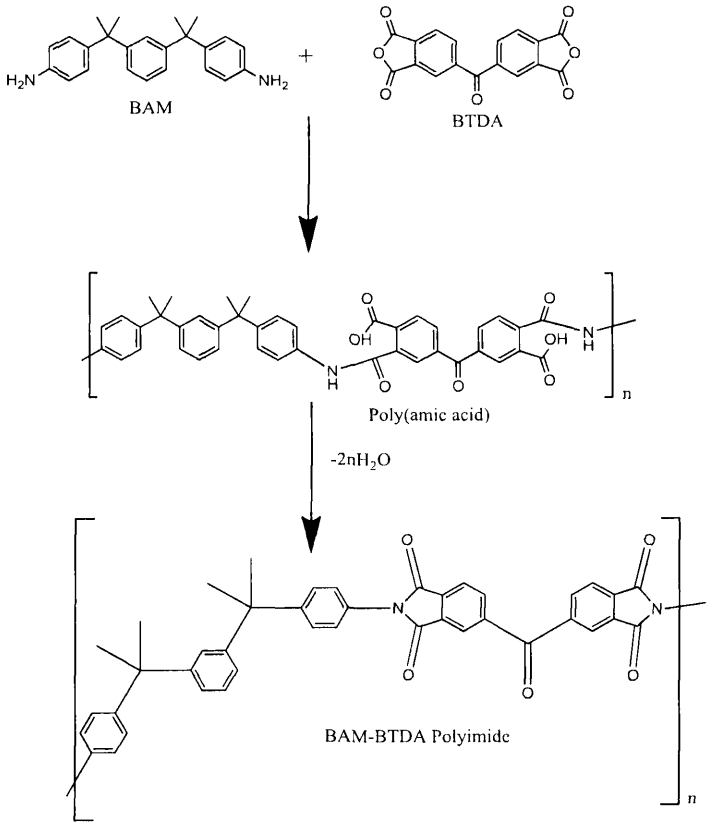

Figure 1: Polyimide synthesis using BAM and BTDA.

The following procedure describes the polymerization of 4,4'-(1,3-phenylenediisopropylidene)bisaniline (BAM) and benzophenone-3,3',4,4'-tetracarboxylic dianhydride (BTDA) in a solvent of *n*-methyl-2-pyrrolidone (NMP). Other diamine and dianhydride monomers as well as other solvents may be used to polymerize under the same protocol.

BAM was received from Aldrich and recrystallized in ethanol (EtOH). The result was an elevation in the melting point range from 107-109°C to 110-111°C. The BTDA was dried in an oven at 135°C overnight to remove any traces of water that may have been present. The monomers were dissolved in solvent prior to the polymerization. 12.02 g BAM (.035 moles) was dissolved in 73 mL of NMP (ρ=1.028 g/mL) and placed inside a 500 mL three-neck round bottom flask equipped with a drying tube and a steady flow of N_2 gas. Next, 11.24 g of BTDA (.035 moles) went into 55 mL NMP and was placed in an addition funnel in the center neck of the reaction flask. The solution in the addition funnel was added dropwise over an hour to the flask while stirring with a magnetic stir bar at room temperature. The polymerization was then allowed to run for 25 hours at room temperature, resulting in approximately 130 mL of poly (amic acid) BAM/BTDA at 15% solution.

The poly (amic acid) was utilized to create film samples. The films were pulled on glass plates with a doctor blade. The glass plates were meticulously cleaned prior to pulling the films, as any dust or residue on the plate is capable of adversely affecting the samples. First the plates were soaked in a base bath. The base bath was made by mixing 200-250 grams of potassium hydroxide into 3 L of isopropyl alcohol in a large glass beaker. After the addition of KOH, 1 L of deionized water was carefully added to the solution. The mixing of this solution is highly exothermic and should not be prepared in a plastic container. After thoroughly rinsing the base off the glass with water, the plate was then scrubbed with soap and water and rinsed with deionized water. Next acetone was applied with a spray bottle to remove any trace amounts of water remaining on the glass and was allowed to dry. The final step in

cleaning the glass plates was a light rinse with ethanol to remove any dust that may have settled on the surface.

After the plate dried, it was placed in the drybox and a film sample was 'pulled' by dragging the doctor blade over a small puddle of poly (amic acid) solution that had been poured onto the plate. The doctor blade was moved firmly, slowly, and consistently over the sample to encourage homogeneity in the film. The sample remained in the dry box at room temperature to allow solvent to evaporate. After the polyamide film had dried to the point where it was not runny but still tacky, typically 18-36 hrs, the glass plate and sample were removed from the drybox and placed in a GS Blue M Electric CW Series Ultra-Temp Oven for curing.

The oven cycles used were varied, but the basic template cycle was 6 steps. First, over an hour the temperature was raised to 100°C and then held there for one hour. Over the third hour of the cycle, the temperature was raised to 200° C and maintained for one additional hour. Finally the temperature was ramped to the cycle's peak temperature of 300°C. This temperature was maintained for a minimum of one hour before cooling to room temperature. During this curing step, the imidization of the poly (amic acid) was completed, taking the sample from the poly (amic acid) to the final polyimide product. The films were removed from the glass plates by soaking them in warm water. At times, vigilant utilization of a razorblade was necessary to remove the films from the plates.

Silver Doped Polyimide Systems

Biological and material degradation are the most obvious harms that are sought to be prevented with these shielding studies, but the aforementioned radiation also can have very deleterious effects on electronics in space. NASA has identified internal electrostatic discharge-based failure in circuit boards as a significant concern for electronics in space applications. A high-energy incident nucleus can impart charge as it passes through any material. If this material is a component of an electrical device, the imparted charge may interfere with the proper function of the component or cause the circuit to short and fail completely. Any data stored on hardware in bits may be altered by excess charges. The solution being proposed is that the typical silicon circuit board be replaced by a polyimide based board that is capable of dissipating excess charges safely away from the working components of the system.

Silver was added to a polyimide to create polymer composites capable of some degree of conductivity. Only partial conductivity is ideal for this application. The poly(amic acid) was synthesized from 4,4-oxydianiline (ODA) and 4,4'-(4,4'-isopropylidenediphenoxy) bis(phthalic anhydride), also known as Ultem dianhydride (UDA), at 10% solution. To incorporate the silver, first a silver complex must be made soluble. Silver (I) acetate (AgOAc) was used, (Aldrich), as in the procedure outlined by Thompson et al. in several published works[9,10,11] and illustrated below.

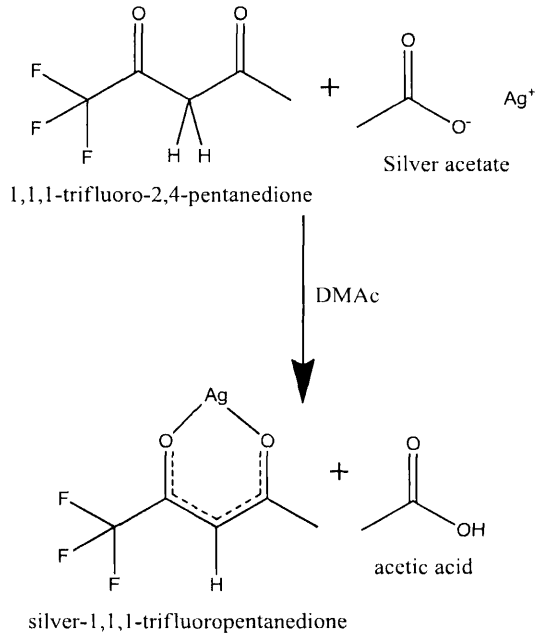

Figure 3: Preparation of the soluble silver complex.

In the first step, 0.381 g (25 *m*mole) of 1,1,1-trifluoro-2,4-pentanedione (TFAH) was combined with 1 mL of dimethylacetamide (DMAc) and 0.306 g (18 *m*mole) of silver acetate (AgOAc) in a small glass container and stirred to yield the silver-trifluoropentanedione complex. An additional .094 g of TFAH were added to create an excess of 1.35 molar equivalents of TFAH (relative to AgOAc), ensuring the formation of all silver into complex. This mixture was slurried for several minutes before the addition of 18.71 g 10% ODA/UDA poly(amic acid), also dissolved in DMAc. The complex solution was soluble in the poly(amic acid) at room temperature. This resin was mixed with a magnetic stir bar for three to five hours before pulling a film in the drybox. The film remained in the drybox at room temperature for a minimum of 18 hours before curing. The polymer was cured in the GS Blue M Electric CW Series Ultra-Temp Oven with the air intake valve closed

completely. This lack of air flow minimized oxidation of the curing film from interaction with air. The oven program previously described in this work for polyimidizations was again implemented, but with the peak temperature of 300°C maintained for 3-5 hours. In the curing process the silver (I) was reduced to metallic silver. This silver reduction is believed to be driven by the presence of electron rich nitrogen and oxygen atoms in the poly (amic acid).

Polyimides were created with different amounts of the silver additive. The equation used to calculate the mass of silver to be added to a given amount of poly (amic acid) for a desired weight percentage is shown below:

$$M_{Ag} = \frac{(\%\, Ag)\left(\frac{MW_{PI}}{MW_{PAA}}\right)(M_{PAA})(\omega_{PAA})}{(100 - \%Ag)}$$

M_{Ag}= mass of silver in polymer

$\%\, Ag$ = mole percentage of silver in the polymer

MW_{PI} = molar mass of repeat unit in polyimide

MW_{PAA}= molar mass of repeat unit in poly (amic acid)

M_{PAA}= mass of polyamic acid in sample

ω_{PAA}= mass fraction of polyamic acid in solution

One must keep in mind that the mass fraction of silver is of interest, even though the silver added to the system is in the form of silver acetate. The mass of silver acetate to be added is found by multiplying the calculated mass of silver by the molar mass of silver acetate and dividing this product by the molar mass of silver. The film samples were made with 3% Ag, 5% Ag, 8% Ag, 10% Ag and 15% Ag by weight.

The resulting film with 3 % Ag by weight exhibited a homogenous luster and reflectivity but also displayed translucence through its deep amber hue. The 5% Ag was homogenously lustrous and reflective. The 8% Ag sample was still lustrous yet barely translucent if at all. A small amount of its surface was covered with a non-reflective, powdery grey finish. In the 10% Ag film, the relative amount of lustrous surface diminished as the grey, non-reflective finish took up a greater percentage of the film's area. In the 15% sample the surface was a marbled outcome of reflective and grey. This sample was also almost completely opaque, tough and appeared more like a metallic foil than a polymer film. It also spontaneously rolled up on itself any time it was not pinned down.

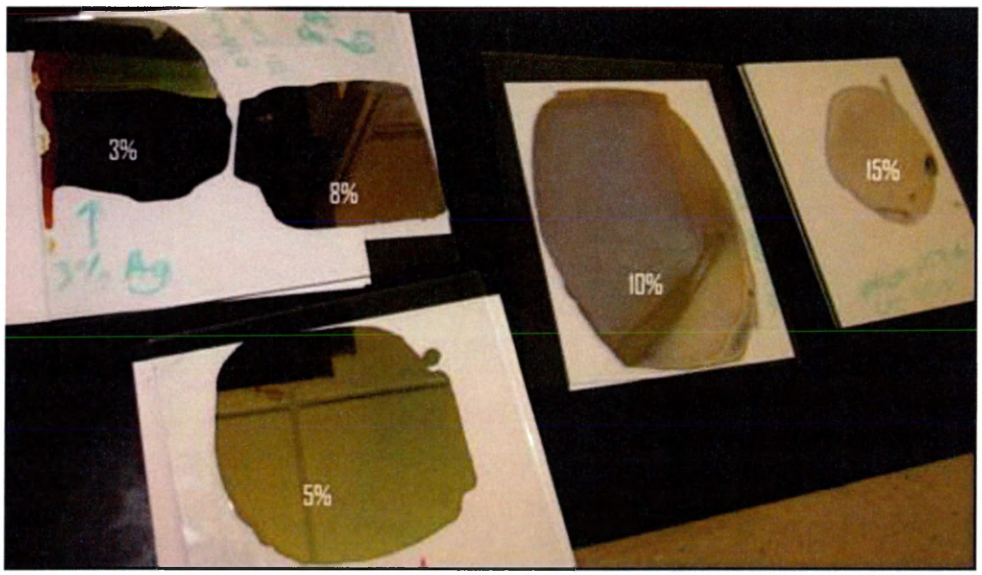

Figure 4: Photograph of the silver doped polyimides after curing.

The most homogenous 4"x4" square areas of the films were matted and cut out of the pulled films to be sent to collaborator at International Scientific Inc. in Radford, Virginia for quantitative conductivity analyses. The luster exhibited by the films does show qualitatively that the silver(I) was reduced, but high reflectivity does not

guarantee any conductivity and vice versa. The conductivity is dependent upon the size and placement of the silver nanoparticles. The resistivities measured by the collaborators at International Scientific Inc. are reported in Table 4.

Sample	Resistivity (Ω-cm)
Kapton Polyimide	$4.47x10^{16}$
UDA-ODA+3% Ag	$1.33x10^{10}$
UDA-ODA+5% Ag	$2.12x10^{9}$
UDA-ODA+8% Ag	$2.32x10^{10}$
UDA-ODA+10% Ag	$6.87x10^{9}$
UDA-ODA+15% Ag	Sample quality insufficient

Table 4: Results of conductivity analysis.

The silvered films were then pressed with other polyimide films to make sample slabs. The films were pressed in a steel mold with an area of 4 inches by 4 inches on a 230 volt 12-ton Carver heated hydraulic Model 4122 press. To fuse the films together, a small amount of solvent was applied to the surface of the film samples before placing them in the press. The resulting silvered polyimide nanocomposite slabs showed excellent fusion of the multiple films and were sent to NASA as deliverables for a Phase I STTR Final Report[12].

Monomer—BDA3 Diamine Synthesis

The synthesis of BDA3 diamine, α,α'-bis3,5-dimethyl-4-(4-aminophenoxy)phenyl]-1,4-diisopropylbenzene, from BDA3-bisphenol through the intermediate BDA3-dinitro was based on previous work by Lucy Y. Hu et al.[13], but had to be modified fairly significantly in some areas. As shown in Figure 2, the conversion to the diamine from the bisphenol was only two chemical steps, but the reduction step was completed using two different pathways. It was found that at almost all steps that the products were not very soluble in anything.

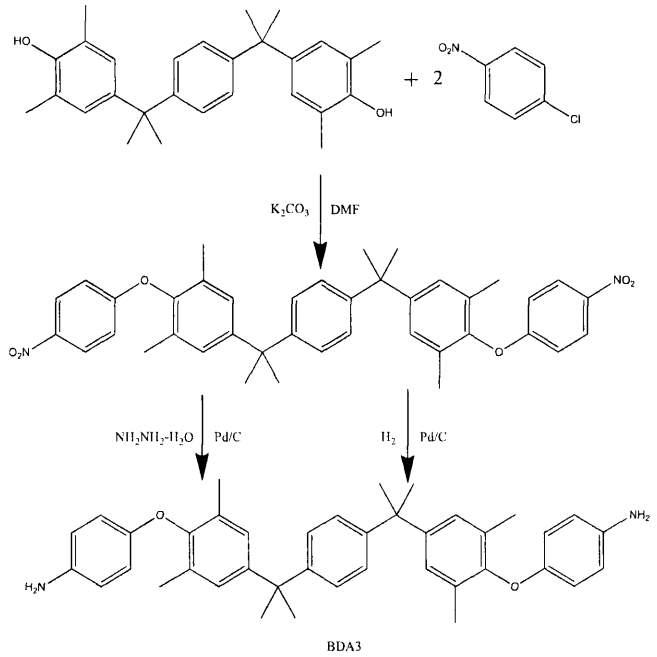

Figure 2: Synthesis of BDA3 diamine monomer.

One such conversion of the bisphenol to the BDA3-$(NO_2)_2$ precursor used 120.90 grams of BDA3-bisphenol (0.30 moles), 104.53 grams of 1-chloro-4-nitrobenzene (0.66 moles), and 91.33 grams of potassium carbonate (0.66 moles) in

500 mL dimethylformamide (DMF). The mixture was stirred in a 2-L, 4-neck flask at refluxing temperature. The initial refluxing temperature was 152-154°C but was lowered to 147-148°C, taken from a thermometer tip in the solution. The reaction was run for 24 hours. The contents of the flask were stirred until cool, at which time they were poured into a 2 L, 50:50 mixture of H_2O and methanol (MeOH) and precipitated. The resulting crystals, bright yellow in hue, were vacuum filtered using a Buchner funnel with trap and further dried in an oven under vacuum at 150° C. The synthesis of the dinitro precursor of BDA3 gave an 88% yield.

For the recrystallization of the BDA3-$(NO_2)_2$ product, glacial acetic acid was initially used but was not an economical solvent due to the large volume required to dissolve a modest mass (<1 gram/100 mL) of BDA3-($NO_2)_2$ at boiling temperatures (~116-118°C). A mixture of toluene and glacial acetic acid was then used with a significant improvement of solubility, but still not good enough to be accepted. The more toluene used, the more soluble the solute was but the products were not always easily crystallized. Finally a solution (no pun intended) was found in acetic anhydride. At very near the boiling point, acetic anhydride quite readily dissolves BDA3-$(NO_2)_2$ at a ratio around 1 gram:10 mL solvent. Usually, the solution was cooled extremely slowly (at a rate of 0.1°C/min) to result in the formation of large dinitro crystals. The hot plate was powered off and the solution was left on the cooling hotplate until it reached room temperature. At this time the solution was placed in the refrigerator. The resulting crystals, while not as large as those cooled in the oven, showed good sharp melting points that agreed well with the literature value[13] of 227-228°C.

An alternate purification of the BDA3-$(NO_2)_2$ product with a sublimation technique was attempted. The bottom of a large sublimator was covered with a layer of the crude dinitro product. The top piece of the sublimator was then put into place, leaving a significant space (approximately 2.5 cm) in between the crude product and the face on which sublimated crystals would be deposited. The sublimator was hooked up to the lab pump, running through the liquid nitrogen trap. The setup was evacuated almost continuously for approximately two days while ice was regularly replaced in the sublimator's cup. The bottom of the sublimation apparatus was placed in an oil bath with temperatures ranging from 130-230°C. After two days, the amount of product sublimated on the inside face was merely a dusting. It is hypothesized that this disappointing trial of sublimation was due to a leak in the evacuated system or insufficient vacuum for sublimation.

Two hydrogenation procedures were used to reduce the BDA3-$(NO_2)_2$ precursor to the desired diamine. Initially, the solvents used by Hu et al.[13] were tried, but solubility of the reactants in the reduction reactions could only be reached to about 10% of their given values. The first used a pressurized hydrogenation setup, with reinforced glassware under heavy agitation and H_2 gas pressurized to approximately 55 psi. An example hydrogenation reaction involved the addition of 15.719 grams of BDA3-$(NO_2)_2$ to 250 mL of a 50:50 mixture of DMF and toluene. Over half, 8.863 grams of the BDA3-$(NO_2)_2$ did not dissolve and was then filtered out, leaving 6.855 grams in the solution, before the addition of 0.520 grams Pd/C catalyst. The reinforced bottle was loaded into the hydrogenation apparatus, purged, pressurized at room temperature with H_2 gas to 55.5 psi and then agitated vigorously.

Approximately 24 hrs later, the pressure had fallen to 47 psi and the apparatus was re-pressurized to 55.0 psi. 36 hours later, the pressure had fallen to 44 psi and was re-pressurized to 56 psi. After another 18 hours, the mixture was removed from the hydrogenation apparatus.

Due to the low solubility of BDA3-$(NO_2)_2$, not even 10 grams of reactant could be used in the hydrogenator system with reinforced bottle. Once again, the solubility ratio was found to be far below that of the literature[13]. Multiple solvents were tried including EtOH, DMF, and tetrahydrofuran (THF). This procedure was abandoned for a second procedure that utilized the addition of hydrazine monohydrate with C/Pd at reflux to reduce the nitro groups.

An example reaction of the aforementioned hydrazine reduction procedure was recorded as follows: 103.48 grams of BDA3-$(NO_2)_2$ (m.p. 227-229°C) was added to 800 mL THF followed by the addition of 0.9402 grams Pd/C catalyst. Next, 310 mL of hydrazine monohydrate were added dropwise over roughtly an hour as the solution was held at reflux (68°C) in a 2-L, 4-neck round bottom flask. The temperature was taken from a thermometer in solution and the system was heated using a 5-L EMV5000/CE electromantle made by Electrothermal. The reaction was allowed to run for 22 hours. This reaction had initially been performed using EtOH as the solvent but was modified to use THF as reported here.

After the reduction of BDA3-$(NO_2)_2$, the very fine Pd/C catalyst must be removed before the product can be isolated. Removal of the catalyst was attempted using Celite pads, glass-sintered funnels, and Buchner filtration methods. The most efficient removal technique utilized a single fine porosity filter paper in a Buchner

vacuum filtration system. If any catalyst remained in the filtrate, the filtration was simply repeated one more time. When removing the catalyst after the hydrazine monohydrate reduction, it was found that the catalyst and subsequently the filter paper were liable to ignite upon reaching dryness. The first discovery of this was in the lab trashcan, not ideal. A procedure was developed whereupon as the final drops of solution were filtering through, deionized water was run through the filter to keep the filter paper wetted. The papers were then stored in a water-filled container kept in the sink to prevent any possible ignition. With the catalyst removed, the product could be obtained. The THF-diamine solution was poured into a 4-L beaker containing 2 L of room temperature water, resulting in the precipitation of final diamine product. The final product was collected and dried and found to be 97% yield. Satisfactory purification of BDA3 has yet to be obtained, but advances were made. The final product's literature value of melting point[13] (226-227°C) was never reached, but after heating samples of the diamine product in an evacuated oven at 215°C for 8 hours, a sharp melting point of 225°C was obtained. Table 3 shows BDA3's solubility in various solvents:

Solvent	**Solubility Notes**
DMAc	Not soluble at RT. Apparently heating caused a chemical change in the BDA3, as observed in a trial recrystallization.
NMP	Somewhat soluble at RT. Did not recrystallize well.
THF	Very soluble. Too soluble for recrystallization.
DMF	Somewhat soluble, more of a suspension.
DMSO	Somewhat soluble, more of a suspension.
CH_2Cl_2	Very soluble almost instantaneous.
$CHCl_3$	Very soluble, almost instantaneous.
EtOH	Not very soluble even upon heating.

Table 3: Solubility of BDA3 in various solvents.

OLTARIS

Introduction and Overview of the Website

OLTARIS, the On-line Tool for the Assessment of Radiation in Space, is an ongoing development by NASA, functioning to assess the behavior of high-energy radiation in space. The coding utilizes the physical modeling programs HZETRN2005 and NUCFRG2. The HZETRN2005 coding simulates high energy transfers of charged nuclei while the NUCFRG2 addresses the events and effect of nuclear fragmentation caused by the incident radiation. OLTARIS is user friendly without the need to be engrossed in the large body of math and physics going into the calculations. It is capable of simulating Galactic Cosmic Radiation and Solar Particle Events as the user sets the parameters for year, duration, and other specifics to the space environment. There are several "space environments" to choose from, such as lunar surface, low-earth orbit, and free-space regions.

The primary interest and focus of this research was on the materials used for shielding. The OLTARIS platform has several standard materials pre-generated and ready to be incorporated such as aluminum, lunar regolith, and polyethylene. The user can define new materials using chemical formulas, elemental weight percentages in a compound, and densities. The parameter inputs are then submitted to generate and configure a database of coding specific to that material. This database can then be used to model the material in radiation exposure simulations, as chosen by the user in the definition of slab layers. The material selected for a layer and the thickness of the layer are submitted through the "slab" or "thickness distribution" tabs. A slab input

simulates just a section of shield at the given depths. The thickness distribution input is much more complex and allows the user to upload possible spacecraft layouts for assessment. Almost all trials outlined in the present document result from use of the slab function tab as the materials and their shielding effects are of priority.

In addition to input options, OLTARIS offers options in its outputs. Most commonly, values are sought in conventions of absorbed dose, measured in milligrays (mGy), and dose equivalent which is measured in millisieverts (mSv). Both have units of J/kg but imply different things. Absorbed dose is a physical measurement of radiation while dose equivalent seeks to quantify the biological effects of radiation. This value is related to the absorbed dose through quality factors which differentiate between different types of radiation (gamma, protons, neutrons, etc.) based on energy. Some forms of radiation are more disruptive and harmful to biological systems, and thus would be weighted more strongly by their respective quality factors. Another quality factor is included for the material under radiation. This factor takes into account a broad spectrum of materials, even specific tissues, organs, and cells[14].

These conversions from dose to dose equivalent may result in non-intuitive results. In a hypothetical example, a measurement of dose was found to be 1 mGy. This same measurement when converted to dose equivalent could be found to have a magnitude much greater, as much as 25 mSv. The difference between the two measurements seems drastic and unrealistic, but it is the biological impact of the radiation dose that is being quantified in sieverts. Sieverts do not represent the physical energy imparted due to radiation but extrapolate the biological effect of this dose. A more thorough explanation of the quantification of biological effects in

conversions to dose equivalence is present in the *2007 Recommendations of the International Commission on Radiological Protection.*[15]

The methods of calculating and simulating such high energy events are continuously being perfected. NASA scientists frequently update OLTARIS to include more thorough and accurate calculations. It even has several outlets for interaction between the users and the group/creators of the website, making it possible to ask questions. For example, during this study a glitch in the software was observed in generating shields with layers of air. The atmospheric composition of air was tabulated as a material and the air layer was incorporated between two blocks of polypropylene. The results showed an increase in radiation over the air interval with a slope of almost one. This increase in permeating radiation was surprising because the number of nuclear fragmentation events should be insignificant in low-density gaseous medium. Because the density of air is extremely low, the resulting thicknesses measured in g/cm^2 were on the order of thousandths. When the same procedure was repeated using hydrogen gas, the increasing effect was not seen and the radiation dropped across the layer of air. These surprising results were identified by the group at NASA Langley as a glitch associated with the super thin layers defined for the air intervals. A solution has since been included in the program. OLTARIS is still deficient in three critical aspects: (1) it is yet to include nuclear cross-sections for neutron absorption by nuclei, (2) the emission of neutrons from nuclear events, and (3) absorption probabilities of the secondary electromagnetic radiation such as gamma rays. This means that the beneficial properties of additives incorporated into shielding

to absorb neutrons or electromagnetic radiation cannot be demonstrated with the current version of OLTARIS.

Basic Material Studies

All simulations on OLTARIS were completed using parameters for a free space environment subject to the GCR of the 1977 Solar Minimum. The materials that have been simulated most with OLTARIS are polyethylene, polypropylene, Kapton polyimide and Ultem 1000 polyimide. Polypropylene and polyethylene have been identified as the two best materials for a single homogenous shield. Their empirical formulas are identical and the only difference observed between the two is a minute change in densities. The shielding success of these two materials is attributed to the fact that they are the most hydrogen-rich polymers. The electron density (electrons/unit mass) of hydrogen is the highest of any element and thus is the best element for absorbing and disrupting such high energy radiation[16].

Table 5 shows the inputs for materials studied. Some of the polymers shown have been included in the table because they were used in studies yet to be discussed and to show the effect of additives on material densities.

Name	Formula	Density
Polypropylene	C_3H_6	0.93 g/cm^3
Polyethylene	CH_2	1.00 g/cm^3
Kapton polyimide	$C_{22}H_{10}N_0O_5$	1.42 g/cm^3
Lead	Pb	11.34 g/cm^3
Tungsten	W	19.25 g/cm^3
Aluminum	Al	2.70 g/cm^3
Kapton+10%Gadolinium	$C_{22}H_{10}N_0O_5$+10%Gd (by wt)	1.55 g/cm^3
Kapton+10%Boron	$C_{22}H_{10}N_0O_5$+10%B (by wt)	1.48 g/cm^3
Ultem 1000	$C_{37}H_{24}N_2O_6$	1.27 g/cm^3
Ultem 1000+10%Gadolinium	$C_{37}H_{24}N_2O_6$+10%Gd (by wt)	1.39 g/cm^3
Ultem 1000+10%Boron	$C_{37}H_{24}N_2O_6$+10%B (by wt)	1.33 g/cm^3
Poly(methyl methacrylate)	$C_5H_8O_2$	1.19 g/cm^3
PMMA+10%Gadolinium	$C_5H_8O_2$+10%Gd (by wt)	1.30 g/cm^3
PDMS+PEI	$C_{26}H_{30}N_2O_7Si_3$	1.18 g/cm^3

Table 5: Inputs for defining materials in OLTARIS.

Single component, monolayer shields were studied first. Figure 4 shows the results of calculations on eleven different materials including the metal tungsten, poly(methyl methacrylate) (PMMA), and poly(dimethylsiloxane)-etherimide (PDMS+PEI) a polymer utilized by collaborators at International Scientific Technologies, Inc. in Radford, Virginia. The results were plotted as the shield thickness in units of areal density, g/cm^2, versus the fractional dose, the ratio of radiation dose measured behind the shield to the radiation incident on the front side of the shield. Areal density measures thickness in terms of mass per unit area. This makes it a great option for comparing materials by taking into consideration the amount of material present in a given thickness. If typical units of length were used, it is likely that many effective materials would be under-evaluated due to differences in their densities.

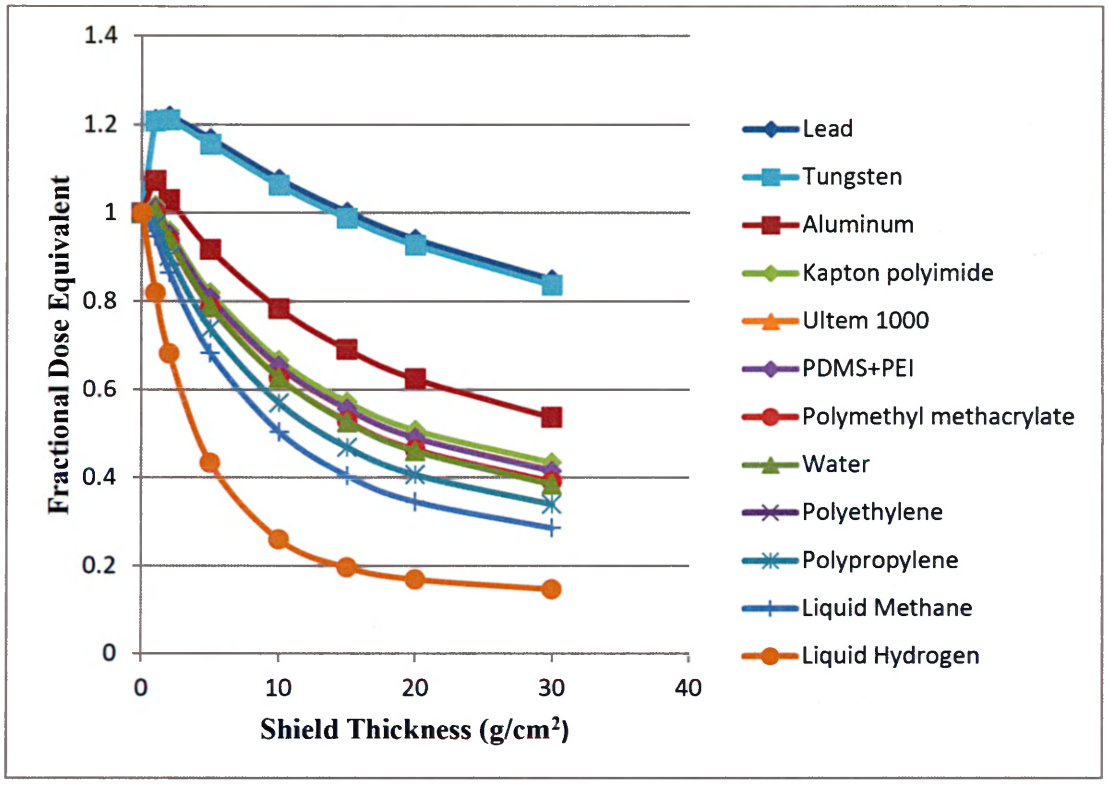

Figure 4: List of materials generated in OLTARIS. Note that the horizontal axis is a measure of shield thickness, not depth into the shields.

Figure 4 shows the radiation as unitless ratios of dose equivalent at the given depth/point relative to the dose equivalent of the incident beam. This is labeled as the "fractional dose equivalent" or H(x)/H(o). For example, the final point (30 g/cm^2) for water was .385 which is equal to 38.5% of the incident radiation. These materials were chosen because they were studied in trials or because they exhibit some standard of a property by which others can be put into a better perspective.

Lead is the best absorber of X-rays but as is apparent in Figure 4, it is a very poor shield for GCR. The best shield was indeed the most hydrogen dense layer possible, liquid hydrogen. This is not a very feasible shield design for spacecraft though, as it would require very complex procedures and systems or unreasonably

large amounts of power to keep properly cooled and in liquid form. Tungsten behaved very closely to lead, with neither showing promise as an effective shield. PDMS+PEI and PMMA both appeared between water and Kapton on the graph, both showing a reduction to about 40% the incident radiation in a 30 g/cm^2 sample. Quite expectedly, liquid hydrogen proved to have the greatest shielding properties of any materials with polypropylene and polyethylene still the best performing polymers. Their performances overlap and are indistinguishable.

All materials exhibit an increase in the relative dose equivalent over some discrete initial interval. This rise in radiation is caused by nuclear fragmentation events between the incident radiation particles and the target nuclei. With increasing atomic number and nuclear size, the probability of these nuclear events also increases. If the relative dose equivalent does not appear to increase for a given material, it is because the initial interval is not small enough to show this effect.

Results and Discussion

The first simulations completed were to show that the outputs were comparable to preexisting data[16]. Polyethylene was an obvious choice, as it was already incorporated into the materials list of the software and could be an integral part of space radiation shielding and infrastructure in the future. It is the most hydrogen-rich polymer, and therefore the best at absorbing and diffusing high energy particles. Other materials tested initially were lunar regolith, also included on the preset OLTARIS materials list, and Kapton polyimide. Figure 5 shows the results.

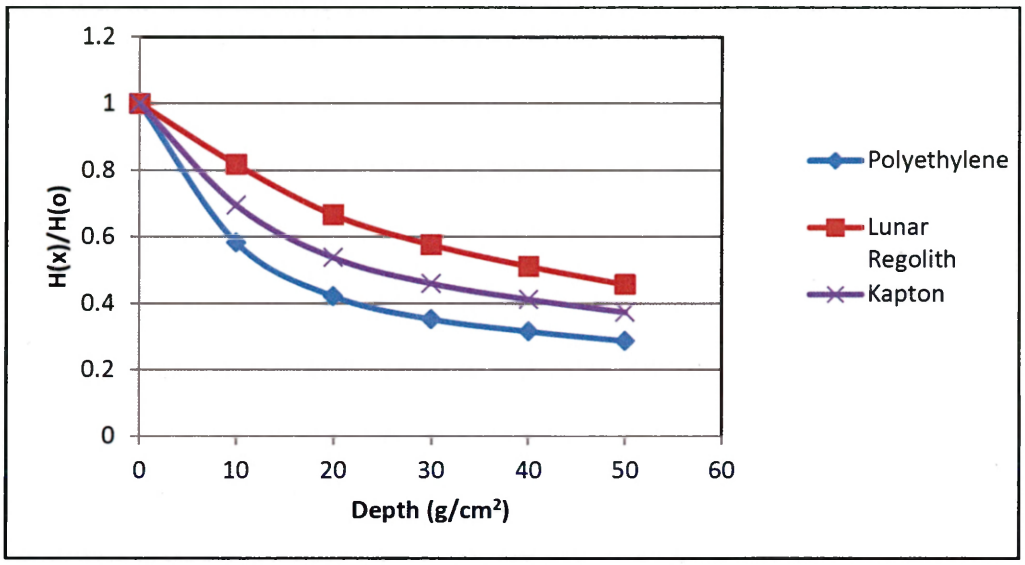

Figure 5: The radiation dissipation vs. depth to compare the OTLARIS output with pre-existing calculations.

According to Kim et al.[16], the relative dose calculated at the backside of a 30 g/cm^2 shield of polyethylene due to GCR is reduced to a value of roughly 30% of the radiation dose experienced without a shield. Initial OLTARIS calculations performed on the same 30 g/cm^2 polyethylene system showed only a 20% reduction in dose. This discrepancy between the OLTARIS calculations and those of the literature was recognized to have resulted from extracting the relative absorbed dose in milliGray from OLTARIS instead of the dose equivalent in milliSievert. When the output parameter was changed, the resulting relative dose equivalent at a thickness of 30 g/cm^2 was calculated to be about 34% that of the incoming radiation. Such a comparison was also completed modeling aluminum.

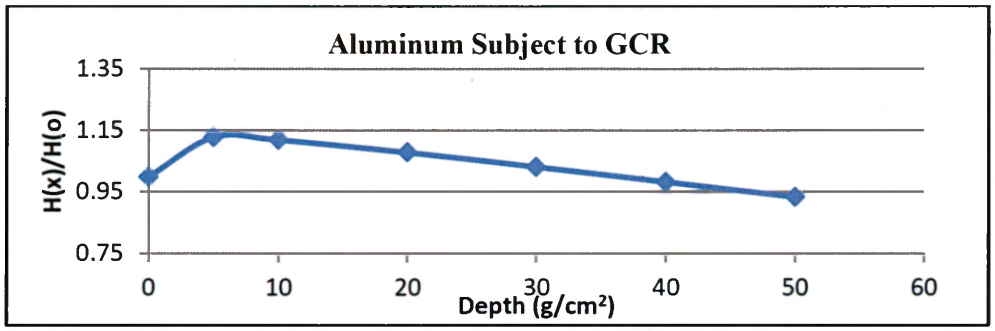

Figure 6: Change in relative dose vs. depth for aluminum subjected to GCR.

Figure 6 was created for comparison with 'Sketch A' in the work also conducted by Kim et al[16]. This agrees with their findings that the absorbed dose increases and reaches a maximum value near 5 g/cm^2 after which it drops off and is also a good example of the variations observed when quantifying dose using different units. The data measured in absorbed dose (Figure 6) spiked to a maximum value and did not decrease below the level of the incident radiation for the first 35 g/cm^2. When the dose equivalence was recorded for aluminum, it increased over a shorter interval and much less dramatically as is shown in Figure 7.

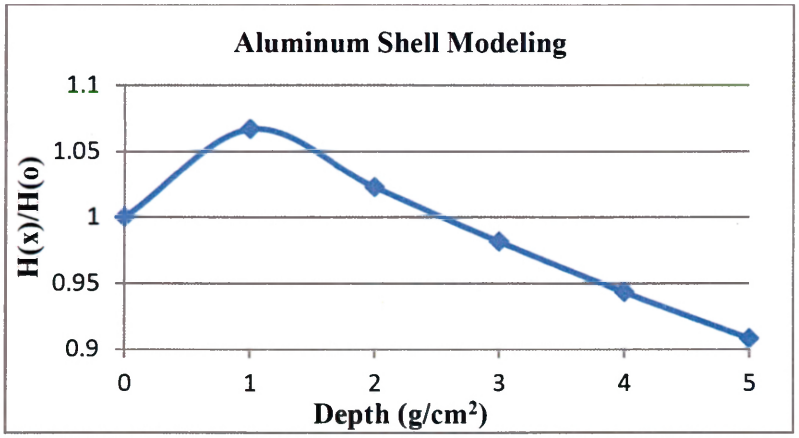

Figure 7: Reduction of relative dose equivalents in aluminum vs. depth in g/cm^2.

These trials reinforce the conclusions that aluminum, at moderate thicknesses, is not an effective shielding material for radiation in space because it interacts with radiation causing internal doses at higher levels than are observed outside the craft[16].

Layered Studies

With polypropylene still setting the benchmark of shielding capabilities, improvement is sought through manipulation of the target slab's composition with multiple layers containing different materials. In OLTARIS, entire shields to be modeled are referred to as 'slabs.' These slabs can be broken down into layers that are individually defined by their thickness and material composition. At the boundary of each layer defined, a calculation is generated for radiation dosage at that depth in the shield. Layers make processing and analyzing the properties of the shield significantly more complex. According to calculations performed with OLTARIS, the addition of more material behind a given point in a shield *decreases* the shielding effectiveness at that given point, regardless of whether the layers are a single substance or are comprised of different substances. The case of a single substance is well illustrated in Figure 8 by Kapton polyimide slabs of increasing thicknesses but always measuring radiation at a point 50 g/cm^2 into the block from the incident radiation.

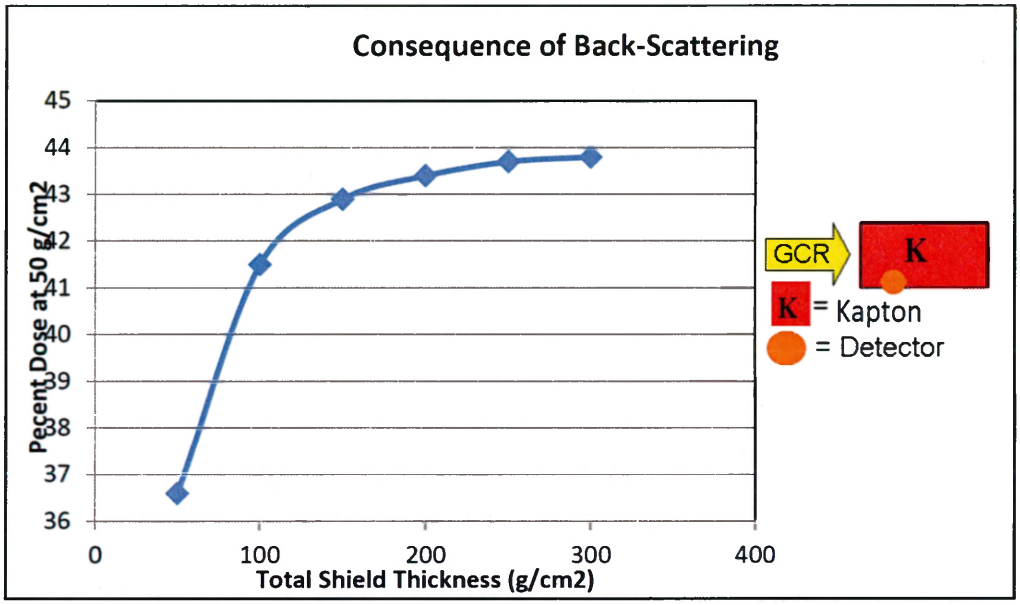

Figure 8: The variable shielding capabilities of the first 50 g/cm^2 of Kapton versus the total thickness of the shields.

As shown in Figure 8, a 50 g/cm^2 polymeric shield alone reduces the incident radiation to about 36.5%. When this layer is placed at the front of a shield with a total thickness of 300 g/cm^2, the incident radiation is reduced to only 43.8% at the constant depth of 50 g/cm^2. This phenomenon persists for all materials tested but is very pronounced with the Kapton polyimide. This effect is apparently a consequence of backscattering by secondary radiation off shielding material behind the detector. The directional momentum must be conserved so the majority of radiation and mass continues through the shield while some projected secondary radiation travels back towards the front of the shield.

The backscattering effect was also strongly evident when another shield was modeled. In this calculation, a 3 g/cm^2 layer of aluminum was positioned in front of a shield to simulate the hull of a spacecraft. This aluminum layer is a known source of

secondary radiation/neutrons resulting from nuclear fragmentation events occurring between the nuclei of the aluminum shell and the incident GCR particles. The increased value of radiation dose at the interface of the aluminum and the front of the shield was used as the value of incident radiation dosage. Behind the aluminum was a 50 g/cm^2 layer of polypropylene followed by a 50 g/cm^2 layer of Kapton polyimide. The calculated dose equivalents were for a detector located at the interface of the two polymer layers. The Kapton layer was doped with varying amounts of gadolinium. Kapton with 50% gadolinium by weight was the highest gadolinium content shield simulated, though it is unclear as to how high of a saturation is feasible. Figure 9 shows the results of the backscatter effect again, but instead of being a function of the total shield thickness, the effect is a function of gadolinium percentage by mass in the Kapton layer.

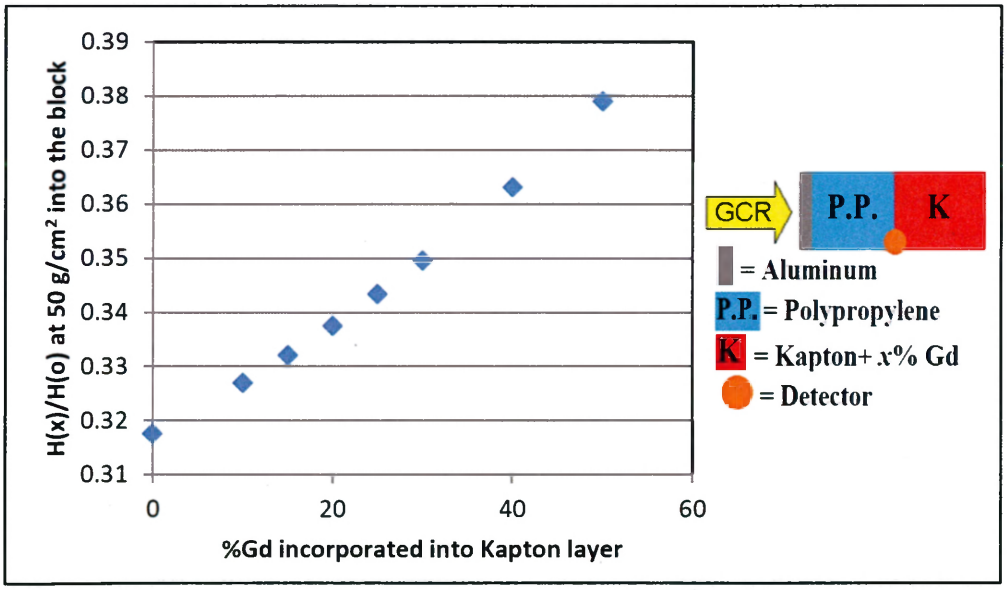

Figure 9: The variable efficiency of shielding at a point located at the interface of the 50 g/cm^2 block of polypropylene and the 50 g/cm^2 block of Kapton as a function of the gadolinium content in the Kapton.

As the amount of gadolinium in the Kapton was increased from 0 to 50 mass percent, the radiation dose equivalent predicted at the front of the Kapton layer was increased from 32% to 38% of that of the incident radiation. The effects of the contents of layers in the slab on other layers closer to the incident radiation are undeniable according to these results, though the reasons are still unclear. They could be simply a function of the polymer density; gadolinium has a rather large influence over this parameter as it is added. These results are also assumed to be described by a simulation that included a scattering of some radiation back towards the front of the shield as it passes through the layers, homogenous or not. The fact that the radiation experienced at a single point inside the shield varies with different compositions does not necessarily describe the overall shielding abilities and effects of the shield as a whole accurately. It was shown that a decrease in shielding at one point in the slab does not mean the system as a whole performs worse. Drawing from these results it is obvious that the materials and their ordering can have dramatic influences over the shielding of a system of layers.

Variable Sequence/Ordering Studies

Simulations of a shield comprising a polypropylene layer and a layer of a second material led to a surprising and consistent conclusion. The shielding capabilities of these systems were found to be better when the polypropylene layer was behind the other layer. This result was always the same, as exemplified with the shields using Kapton or Ultem 1000 as the second material. Shown below in Figure 10, trials with two layers, one Kapton and one polypropylene, were on average 7-8%

more effective in reducing incident GCR when the Kapton layer was in front. Similar results were also found in trials completed with the metallic additives of gadolinium and boron incorporated into the polymers.

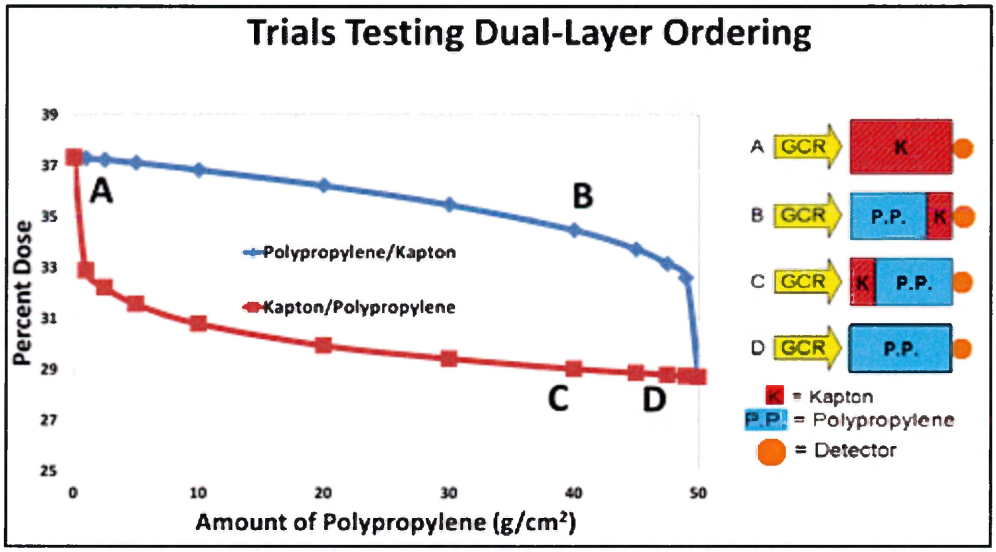

Figure 10: Effects of layer ordering. The horizontal axis shows the composition of polypropylene in a standard 50 g/cm^2 thick shield.

The data plotted above were the radiation values at the backside of a 50 g/cm^2 shield. The composition and ordering of the Kapton and polypropylene layers in the shield were varied, but the total slab thickness of 50 g/cm^2 was held constant through the trials. The data show what a significant effect even a 2% composition change or ordering can have. The shielding efficiency is shown to be much better when the Kapton layer is the front layer, for a given thickness of polypropylene. A turning point in this graph appeared near the hyperbolic endpoints, at the proportions of 1:49 g/cm^2 between the layers. Pure, homogenous polypropylene is the optimal shield for 50 g/cm^2 of material, but when just one g/cm^2 polypropylene is incorporated after 49 g/cm^2 of Kapton, the shielding abilities of the slab are predicted to be significantly

enhanced than those of pure Kapton. In fact the shield would be closer in quantitative shielding capabilities to a pure polypropylene shield than one of pure Kapton. This is a surprising result considering the system of slabs is 98% Kapton. Note that 49 g/cm^2 of Kapton followed by 1 g/cm^2 of polypropylene is almost equivalent in shielding to 49 g/cm^2 polypropylene followed by 1 g/cm^2 of Kapton with the difference in radiation reduction effectiveness only being 0.2-0.3%. This is a very intriguing result considering the 8% difference in shielding between pure polypropylene and pure Kapton over a 50 g/cm^2 block.

Variable Shielding Efficiency

Another observation consistent for shields of multiple layers comprised of polypropylene and another material occurs only when the polypropylene is the more deeply embedded material. In this scenario, polypropylene's contribution to shielding efficiency is dependent upon the material in front of it. This is true both in Kapton/polypropylene and poly(methyl methacrylate)/polypropylene slabs as well as with shields of compositions containing variable additive concentrations in the first layer of the slab. An example of such a system can be seen below in Figure 11 with Kapton and polypropylene.

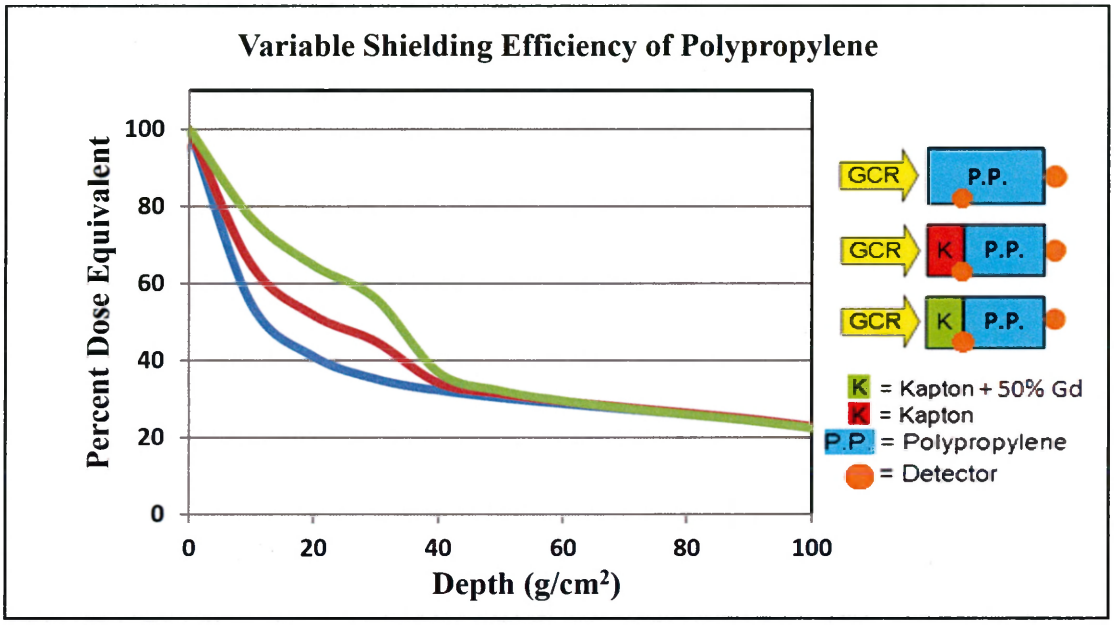

Figure 11: The percent ratio of radiation dose equivalent to incident radiation dose equivalent vs. the detectors' depth of the shield. The shield composition for the trials, 30 g/cm^2 of Kapton(+Gd) followed by 70 g/cm^2 polypropylene all preceded by a 3 g/cm^2 aluminum shell.

Figure 11 depicts a system of layers where, as the percent gadolinium content percentage increased, the radiation experienced behind the shield was barely affected. A similar result was also seen when PMMA was used in place of Kapton but the data spanned a narrower range. This reduced range was due to limitations involved with heavy metal incorporations into PMMA as outlined in the patent by Johannes Smid[17]. The PMMA was only tested with gadolinium contents up to 30% by weight whereas the Kapton was tested with up to 50% gadolinium.

Another experiment revealed that when the order of the layers seen in Figure 11 was reversed, there was a significant difference in shielding. Figure 12 depicts a plot of radiation shielding versus the gadolinium content of the PMMA layer and compares the ordering of the layers in the slab.

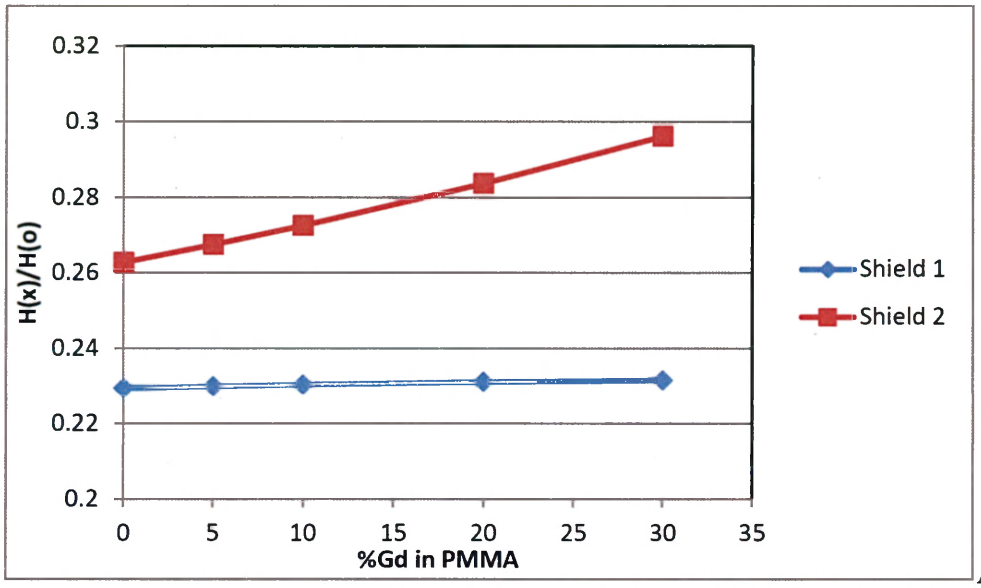

A.)

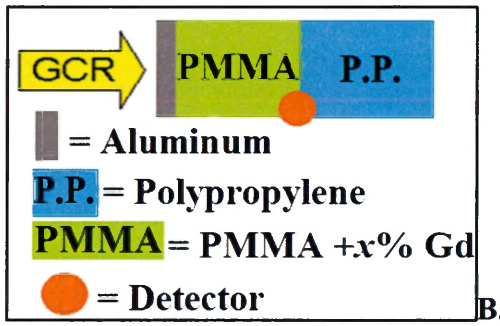

B.)

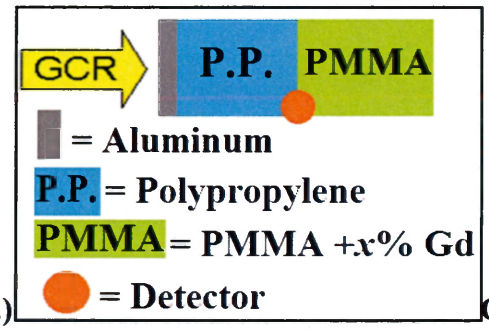

C.)

Figure 12: A) Fractional dose versus % incorporation of Gd in the PMMA layer. B) depiction of shield 1, C) depiction of shield 2. In these shields, both the PP and PMMA+*x*% Gd layers are each 50 g/cm^2.

It is evident from Figure 12 that the preferred ordering for the slab is with the PMMA or PMMA+Gd layer positioned in front of the polypropylene layer. The negative effects of the gadolinium were greatly reduced when polypropylene was positioned behind the gadolinium-loaded PMMA. The difference in relative dose behind the shield is only about 3% in the absence of gadolinium and grows to about 7% with 30% gadolinium by mass incorporated into the PMMA layer. All simulations of dual-layered systems that have included polypropylene as one of the layers have yielded the same results.

Foil versus Dispersion Incorporated Additives

The metals sought to be added to the polymers for the absorption of secondary radiation (gadolinium, boron and tungsten) can be obtained both as foils and as powdered nanoparticles. The foil would be a thin metal layer in the system while the powder must be dispersed (as homogenously as possible) throughout polymer slab. Achieving a thoroughly homogenous doping of a polymer layer may be much more synthetically complex and difficult than just placing a foil between two layers in the slab. Figure 13 shows one system of layers including polypropylene and UDA-BAM with 10% tungsten nanoparticles (by mass) incorporated into the polymer matrix compared to three trials of similar layered systems including tungsten as a pure element thin film in the ordering of polymeric slabs. The final shield was composed of polypropylene and pure UDA-BAM with no tungsten added. Tables 6 and 7 provide descriptions of the five multi-layered systems. Each of the shields with tungsten had the same total mass of tungsten incorporated either as a powder or a foil.

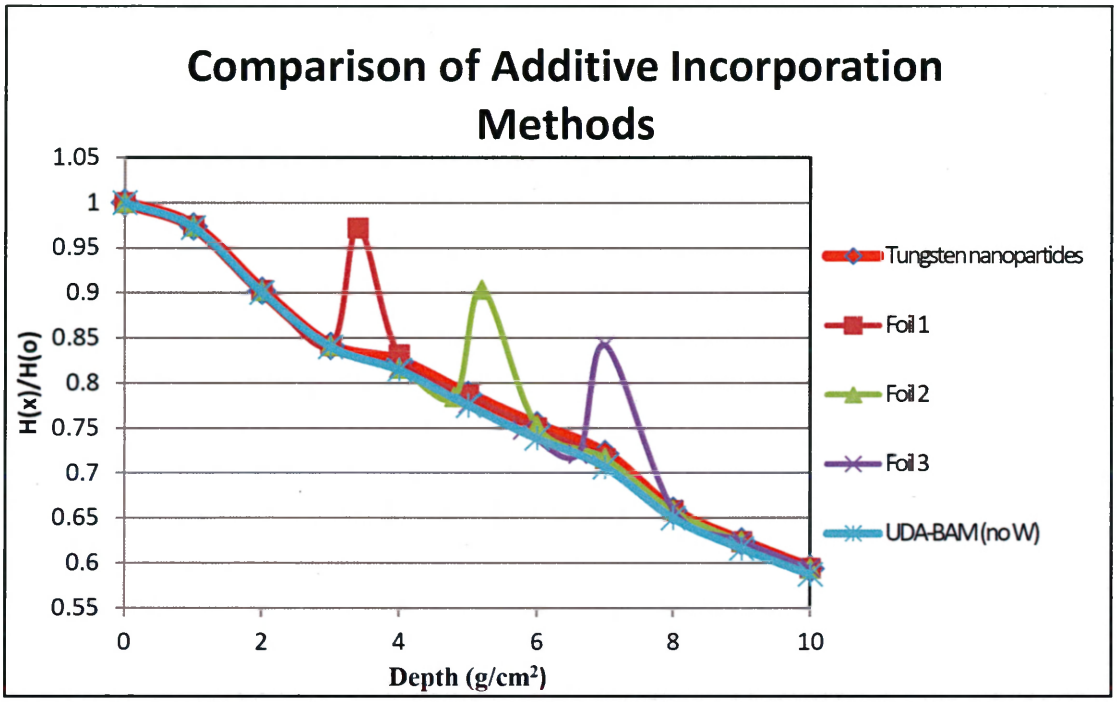

Figure 13: Comparison of polymeric systems with W foil and dispersed nanoparticles.

Depth g/cm^2	Tungsten Nanoparticle	UDA-BAM (no W)
0-1	P.P.*	P.P.
1-2	P.P.	P.P.
2-3	P.P.	P.P.
3-4	UDA-BAM +10%W	UDA-BAM
4-5	UDA-BAM +10%W	UDA-BAM
5-6	UDA-BAM +10%W	UDA-BAM
6-7	UDA-BAM +10%W	UDA-BAM
7-8	P.P.	P.P.
8-9	P.P.	P.P.
9-10	P.P.	P.P.

Table 6: Compositions of shields (Figure 13) including UDA-BAM with tungsten nanoparticles and pure UDA-BAM with no tungsten added. *Polypropylene

Foil 1		Foil 2		Foil 3	
Depth g/cm^2	**Layer**	**Depth g/cm^2**	**Layer**	**Depth g/cm^2**	**Layer**
0-1	P.P.	0-1	P.P.	0-1	P.P.
1-2	P.P.	1-2	P.P.	1-2	P.P.
2-3	P.P.	2-3	P.P.	2-3	P.P.
3-3.4	W Foil	3-4	UDA-BAM	3-4	UDA-BAM
3.4-4	UDA-BAM	4-4.8	UDA-BAM	4-5	UDA-BAM
4-5	UDA-BAM	4.8-5.2	W Foil	5-5.8	UDA-BAM
5-6	UDA-BAM	5.2-6	UDA-BAM	5.8-6.6	UDA-BAM
6-7	UDA-BAM	6-7	UDA-BAM	6.6-7	W Foil
7-8	P.P.	7-8	P.P.	7-8	P.P.
8-9	P.P.	8-9	P.P.	8-9	P.P.
9-10	P.P.	9-10	P.P.	9-10	P.P.

Table 7: Layered slab compositions, shown in Figure 13, for comparison of additive incorporation.

The peaks in the curves correspond to the layer of tungsten foil. The system simulated with tungsten nanoparticle dispersion remains, for the most part, on the lowest lying line and does not exhibit positive slope between any data points. The final calculated values of radiation dampening behind 10 g/cm^2 of these shields varied by only a fraction of a percent. This result shows that how the tungsten is incorporated into the a polymeric slab may be trivial from the perspective of effective shielding capabilities and a preference between incorporation methods would be made based on the specific physical requirements of the application and further testing on secondary radiation absorption capabilities.

Complex Multi-Layered Systems

OLTARIS simulations have been implemented to analyze and characterize polymeric radiation shielding with the intent of designing an enhanced shield capable of sufficiently reducing deleterious effects of the high energy radiation incident in the space environment. To achieve this shield, a multi-layered polymeric system is hypothesized to be the most effective route.

To shield against GCR nuclei, it is believed that a hydrogen-rich polymer is particularly effective in slowing the incident radiation through Coulombic interactions while keeping the shield's mass low. For this application, polypropylene and polyethylene are both well suited. Polypropylene was chosen over polyethylene however, because of its greater thermal and mechanical properties[5,6]. The secondary radiation components that are created in nuclear fragmentation events between the shield and GCR must also be targeted. Included among the nuclear fragments are secondary neutrons. Thus, boron additives will be utilized for their high neutron-capture cross sections in polyimide slabs.

Tungsten is incorporated into polyimide layers to promote the absorption of secondary electromagnetic radiation. The metal additive may also enhance the polymer's physical structural integrity. With its high atomic number, it is expected that incorporated tungsten will be especially susceptible to nuclear fragmentation events with GCR. This prediction, coupled with the reoccurring results of many material ordering experiments (see Figures 8, 9 and 10), led to the designation of the

final material layers in the multi-layered shielding system as polypropylene. A schematic summarizing the basic model is shown below in Figure 14.

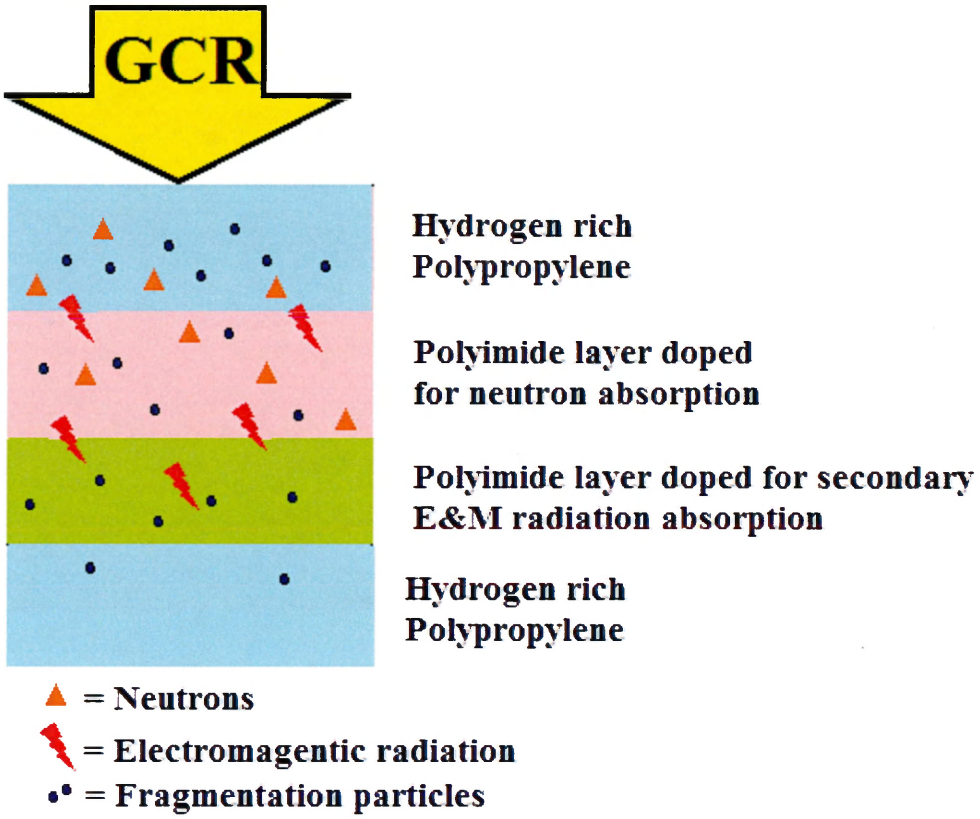

Figure 14: schematic of optimized multi-layered polymeric shield.

Trials analyzing variable multilayered systems were conducted to compare effectiveness in layer ordering and placement in the shield. Figure 15 shows the results of these first trials, converted from dose equivalent in mSv/day to the unitless quantification of H(x)/H(o). Each data point is equated to a detector imbedded at a given depth in the shield.

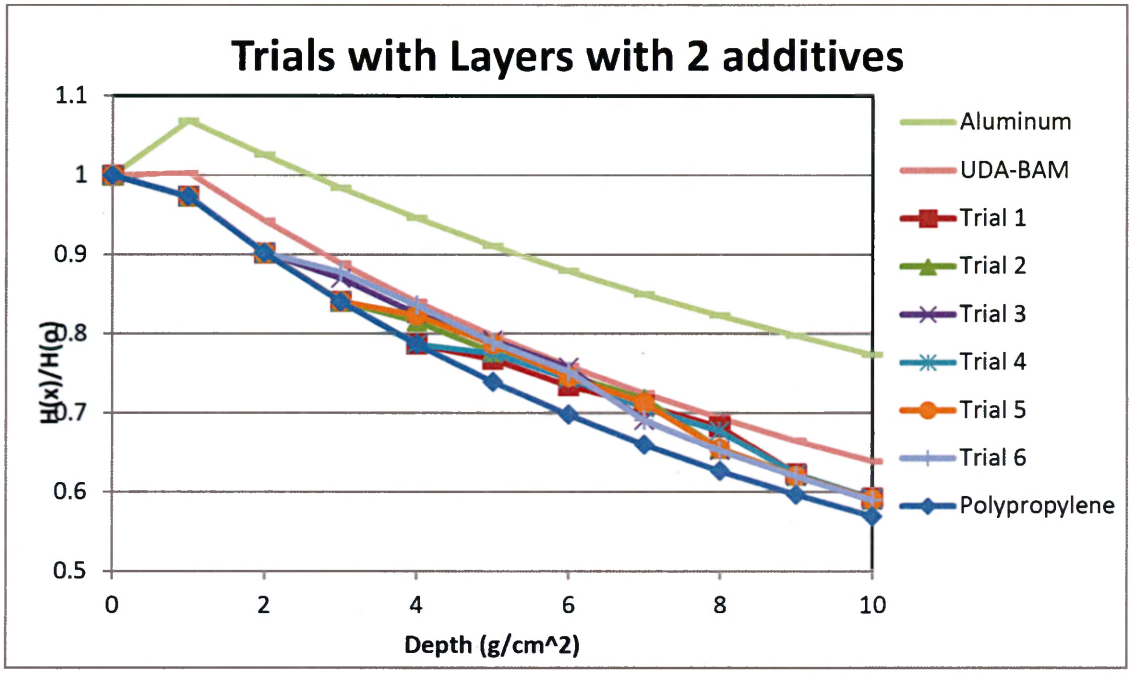

A)

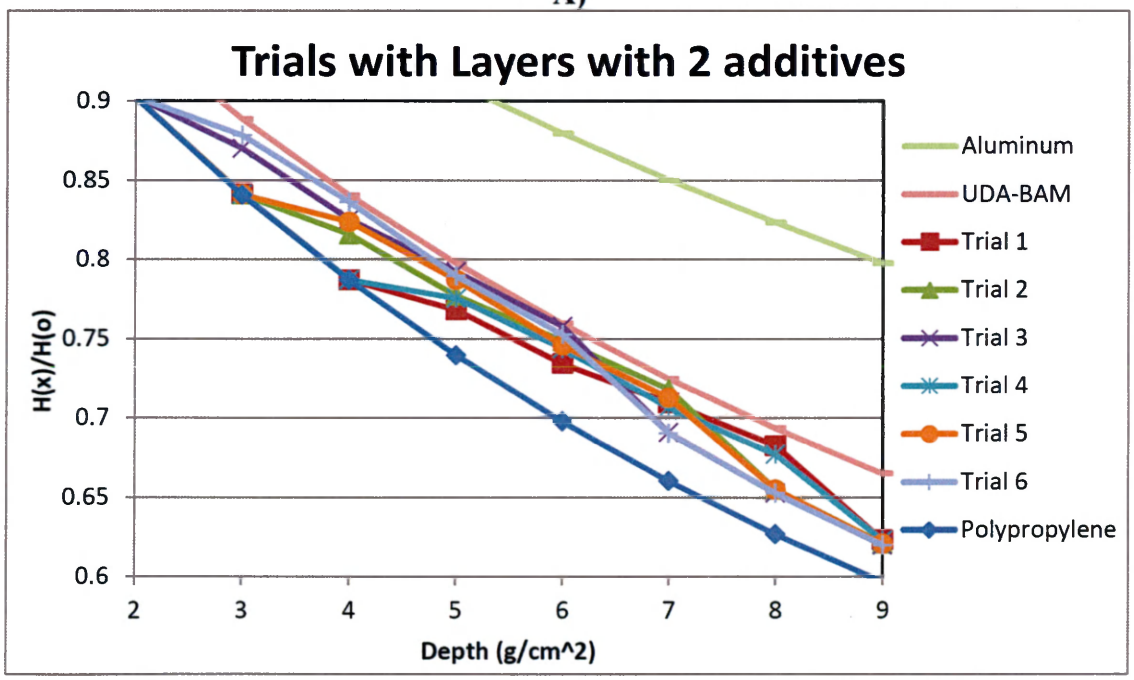

B)

Figure 15: A) Evaluation of multilayered trials, compared to pure aluminum, UDA-BAM, and polypropylene. B) Close up of the area where the results of multilayered trials diverge.

Tables 8 and 9 depict the multilayered systems evaluated in Figure 15.

Depth (g/cm^2)	Trial 1	Trial 2	Trial 3
0-1	Polypropylene	Polypropylene	Polypropylene
1-2	Polypropylene	Polypropylene	Polypropylene
2-3	Polypropylene	Polypropylene	UDA-BAM+10%B
3-4	Polypropylene	UDA-BAM+10%B	UDA-BAM+10%B
4-5	UDA-BAM+10%B	UDA-BAM+10%B	UDA-BAM+10%W
5-6	UDA-BAM+10%B	UDA-BAM+10%W	UDA-BAM+10%W
6-7	UDA-BAM+10%W	UDA-BAM+10%W	Polypropylene
7-8	UDA-BAM+10%W	Polypropylene	Polypropylene
8-9	Polypropylene	Polypropylene	Polypropylene
9-10	Polypropylene	Polypropylene	Polypropylene

Table 8: The multilayered compositions of Trials 1-3 shown in Figure 15.

Depth (g/cm^2)	Trial 4	Trial 5	Trial 6
0-1	Polypropylene	Polypropylene	Polypropylene
1-2	Polypropylene	Polypropylene	Polypropylene
2-3	Polypropylene	Polypropylene	UDA-BAM+10%W
3-4	Polypropylene	UDA-BAM+10%W	UDA-BAM+10%W
4-5	UDA-BAM+10%W	UDA-BAM+10%W	UDA-BAM+10%B
5-6	UDA-BAM+10%W	UDA-BAM+10%B	UDA-BAM+10%B
6-7	UDA-BAM+10%B	UDA-BAM+10%B	Polypropylene
7-8	UDA-BAM+10%B	Polypropylene	Polypropylene
8-9	Polypropylene	Polypropylene	Polypropylene
9-10	Polypropylene	Polypropylene	Polypropylene

Table 9: The multilayered compositions of Trials 4-6 shown in Figure 15.

The results show that pure polypropylene is the most effective shield for GCR. The multi-layered compositions (Trials 1-6) were not significantly worse in this analysis, on average they shielded 2.16% [H(x)/H(o)] less effectively than the polypropylene control with a standard deviation among the six trials of only 0.11%. There was no difference of shielding capabilities observed in the relative ordering between the UDA-BAM+10% B layers and those with 10% W. While the multi-layered shields are shown to be inferior to pure polypropylene, the full effects of the beneficial properties sought in the additives (the absorption of secondary

electromagnetic radiation and free neutrons) are not yet accounted for in OLTARIS's simulations.

To better model the shielding environment for applications inside a spacecraft, experiments were repeated on the multi-layered Trials 1-3, but placed behind a 2 g/cm^2 slab of aluminum to simulate the hull of such a vessel. These new multilayered trials' compositions are shown in Table 10.

Depth (g/cm^2)	Trial Al 1	Trial Al 2	Trial Al 3
0-1	Aluminum	Aluminum	Aluminum
1-2	Aluminum	Aluminum	Aluminum
2-3	Polypropylene	Polypropylene	Polypropylene
3-4	Polypropylene	Polypropylene	Polypropylene
4-5	UDA-BAM+10%B	Polypropylene	Polypropylene
5-6	UDA-BAM+10%B	UDA-BAM+10%B	Polypropylene
6-7	UDA-BAM+10%W	UDA-BAM+10%B	UDA-BAM+10%B
7-8	UDA-BAM+10%W	UDA-BAM+10%W	UDA-BAM+10%B
8-9	Polypropylene	UDA-BAM+10%W	UDA-BAM+10%W
9-10	Polypropylene	Polypropylene	UDA-BAM+10%W
10-11	Polypropylene	Polypropylene	Polypropylene
11-12	Polypropylene	Polypropylene	Polypropylene

Table 10: Multilayered compositions of Trials Al 1-3.

Qualitatively, it is expected that the incident GCR will have a significantly increased rate of nuclear fragmentation with the target aluminum nuclei, thus subjecting the polymeric layers to greater secondary radiation. Figure 16 shows the results of calculations on trials with the aluminum shell, as shown in Table 10, and also includes pure shields of aluminum, UDA-BAM, and polypropylene for comparison.

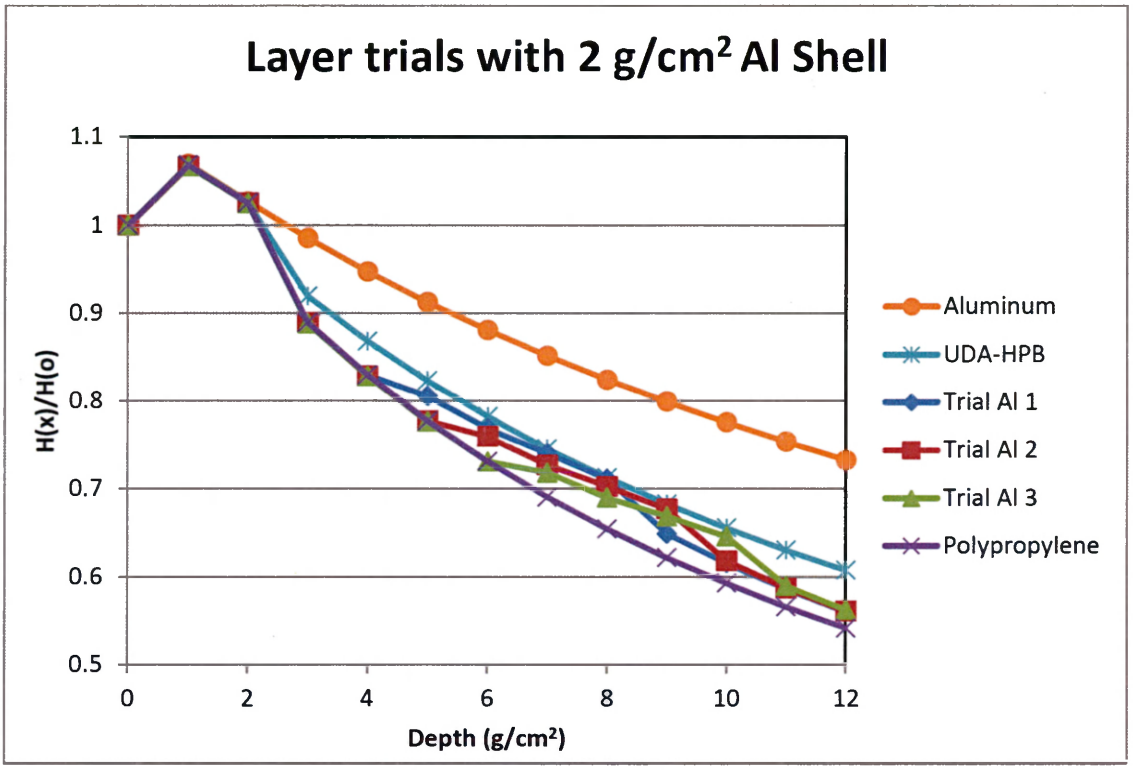

Figure 16: Multilayered trials including an aluminum shell preceding the polymer layers. The compositions of the multilayered trials are shown in Table 9.

The most intriguing observation is the notable increase in the shielding efficiencies of the polymer layers directly following the aluminum. The amount of radiation dose equivalent reduction per unit thickness is greater in the first polymer slab of a shield than over any of the other intervals. The average value of H(x)/H(o) behind the shield for the three multi-layered trials was 56.1% (standard deviation of 0.119%) with the incident radiation being reduced to 52.8% through the polypropylene slab. The three trials varied only by the placement of the six 1 g/cm^2 polypropylene layers. None of these multi-layered slabs reduced radiation significantly more than the others. In comparison to pure polypropylene, the multi-layered systems were only slightly less effective in shielding according to the

OLTARIS calculations, while their intended benefits of secondary radiation absorption and improved mechanical properties must be shown through other experimental methods. Updates to include the absorption of neutrons and gamma rays and further analysis would be expected to show an increase in the performance of the proposed multi-layer shielding systems.

MISSE-X Modeling

All OLTARIS simulations have been conducted in a free space environment, to mimic the conditions of long distance, interplanetary space flights. However, very few manned missions have ever been outside of low Earth orbit (LEO). Currently, the International Space Station (ISS) maintains low Earth orbit at an altitude range of 378-460 kilometers at an inclination of 51.6° relative to the equator. This places the craft in the protective electromagnetic sphere of the Earth and the Van Allen Belts, Figure 17.

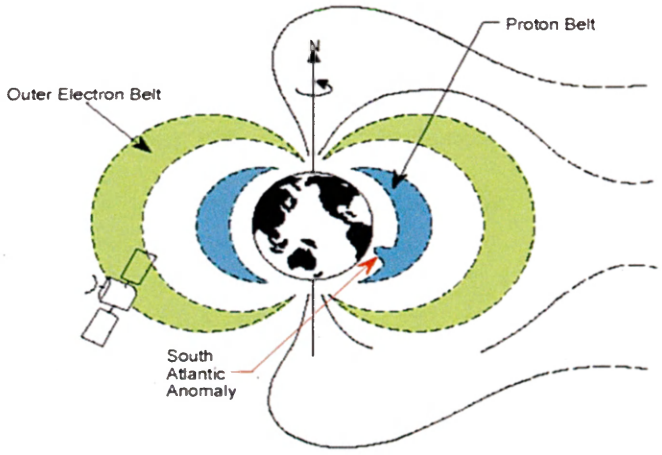

Figure 17: Trapped Radiation Belts Around Earth[18].

The Earth's fields trap incoming charged particles in two belts. The outermost belt consists of mostly electrons and the inner belt collects other charged particles, mostly protons. Also shown in Figure 17 is the South Atlantic Anomaly. This is where the inner belt of charged matter reaches its lowest altitude and correspondingly where the ISS experiences the most intense radiation in its circular orbit.

MISSE-X, Materials on the International Space Station Experiment-X, is a proposed collaboration of experiments for materials subject to the LEO space environment to be implemented externally on the ISS. There have been multiple MISSE missions since the original MISSE was placed on the ISS in August of 2001[19]. Most of the MISSE experiments to date have been passive, requiring the return of the materials to Earth to be analyzed. As the post-shuttle era has commenced, MISSE-X will be the first MISSE platform to emphasize active sensing and monitoring of the external space environment.

An experiment has been proposed by International Scientific Technologies, Inc. in conjunction with the College of William and Mary. The experimental volume is expected to be limited to a four inch cube located on the MISSE-X platform. This volume must contain the material being tested for its shielding capability and its sensing apparatus, a dosimeter. To better comprehend what is expected from the proposed experiment, several systems were modeled using OLTARIS. The OLTARIS calculations were carried out in free space and low Earth orbit environments of 1977, the year of recorded maximum in GCR exposure.

So far, all OLTARIS calculations shown have utilized slab geometry modeling. These models limit the simulations to a two-dimensional analysis of the

materials subjected to incident radiation from one direction. However, OLTARIS does allow one to model complicated three-dimensional arrangements of materials by uploading a user defined thickness distribution in XML format. In these simulations, the system was a basic sphere of 3 inch radius with the final depth being the center of the shield's core. To define this spherical shield, a ray distribution was used. Rays are vector lines that are defined by their origin location, three dimensional direction, and length. The website has multiple ray distributions available to users ranging from distributions of 42 to 10,000 rays. In this study, a ray distribution defining 1,002 rays was utilized in the XML coding to model the three inch spheres. The results of four modeled spheres of polymeric materials subject to free space and low Earth orbit are shown below in Figure 18 with the accompanying Table 11 displaying the dose equivalent reduction as calculated using OLTARIS.

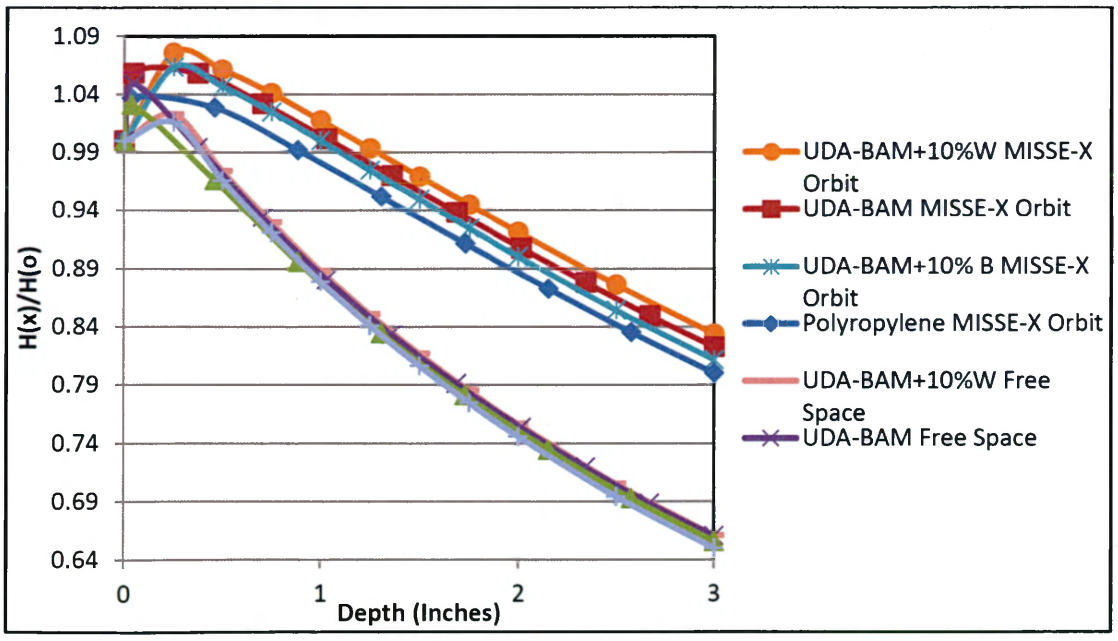

Figure 18: Comparison of shielding performance in LEO and free space.

Material	Free Space	MISSE-X
Polypropylene	34.44%	19.98%
UDA-BAM	33.98%	17.74%
UDA-BAM+10%B	35.02%	18.84%
UDA-BAM+10%W	33.94%	16.62%

Table 11: Percentage reduction in radiation dose equivalence over the 3 inch spherical shields.

Figure 18 compares the materials using a length measurement, inches, rather than areal density as the other OLTARIS calculations have been reported. Because the proposed MISSE-X experiment must be contained within the specified volume, areal density was not of importance to this study. In the Free Space calculations, it was found that UDA-BAM+10%B was expected to slightly outperform polypropylene. This result is an effect of using length instead of areal density in the definition of shield depth.

The results most blatantly show that the materials used in the calculations are much more effective in shielding radiation in the Free Space environment. This result is due to the large difference in incident radiation values, H(o), between the two environments. Radiation incident on the systems modeled in free space was greater than that incident on systems in low earth orbit by over a factor of eight. It is not surprising to find that the shields subject to more radiation are capable of greater relative shielding. It is surprising however to note that the initial increase in observed fractional dose due to interactions of the incident radiation and the shielding material is greater in the low Earth orbit shields.

CONCLUSIONS

The radiation outside of the Earth's geomagnetic sphere is expected to have hugely detrimental effects on biological systems as well as electronic equipment. Until sufficient shielding of radiation present in the space environment is reached, long-termed manned missions in deep space are not feasible. Materials capable of protecting space craft through significant radiation reduction are expected to be lightweight polymers. Over the course of this work, research was conducted in polymer synthesis as well as in modeling and simulation of the radiation effects on materials subject to GCR and LEO.

The synthetic approach focused on the utilization of polyimides for shielding applications. A fairly hydrogen-rich diamine monomer, BDA3, was successfully synthesized and its synthesis procedure streamlined from previous work. Complications from the low solubility of BDA3 and its corresponding polymer have, so far, resulted in films of low quality. Several polyimides were successfully synthesized from poly(amic acid)s comprised of several different diamine and dianhydride monomers. Silver was incorporated successfully into polyimide films for the intended application of mitigating electrostatic discharge on the surface of circuit boards in space.

The modeling program OLTARIS was used for studying shielding systems subject to space radiation. Individual materials were evaluated for their relative shielding effectiveness. Layered systems of materials were studied to identify key relationships and effects present. Every test has shown that any layer in a system has an influence on the shielding performances of the other layers both before and after it.

Observations of variable ordering in layer placement on shielding effectiveness heavily guided the development of new systems. A multi-layered system of polymeric materials designed to target and reduce specific components and products of GCR has been proposed and evaluated with OLTARIS. OLTARIS was also used to study the differences between the low Earth orbit and free space environments for future evaluations of polymeric radiation shields with the MISSE-X program.

Continuing research is necessary in both polymer synthesis and theoretical modeling of materials in space environments. The research and production of new polyimides of high hydrogen content and improved mechanical and physical properties will remain a focus of material development for these applications. Further analysis of the proposed multi-layer polymeric shielding systems is necessary to more accurately describe its effectiveness. Experiments observing the absorption of neutrons and electromagnetic radiation that result from interactions of the GCR with the shielding materials are adding to our understanding by supplementing the OLTARIS modeling which cannot account for neutrons and electromagnetic radiation.

REFERENCES

[1] Churchill, R.; Aquino, E.; Orwoll, R.; Kiefer R., "Multilayered Polymeric Shielding to Protect Humans from Galactic Cosmic Radiation," NASA Phase II Proposal, 2010.

[2]Guetersloh, S.; Zeitlin, C.; Heilbonn, L.; Miller, J.; Komiyama, T.; Fukumura, A.; Iwata, Y.; Murakami, T.; Bhattacharya, M., "Polyethylene as a radiation shielding standard in simulated cosmic-ray environments," *Nuclear Instruments & Methods in Physics Research, Section B: Beam Interactions with Materials and Atoms*, **252(2)**, 319-332 (2006).

[3] Reitz, Guenther, "Characteristic of the radiation field in low Earth orbit and in deep space," *Z. Med. Phys.* **18**, 233–243 (2008).

[4] Wilson, J. W.; Denn, F. M, "PRELIMINARY ANALYSIS OF THE IMPLICATIONS OF NATURAL RADIATIONS ON GEOSTATIONARY OPERATIONS," NASA Technical Information Service, NASA TN D-8290 (1976).

[5] Dynalab Corp, "Plastic Properties of High Density Polyethylene," November 28, 2012. <http://www.dynalabcorp.com/technical_info_hd_polyethylene.asp>.

[6] Dynalab Corp, "Plastic Properties of Polypropylene," November 28, 2012. <http://www.dynalabcorp.com/technical_info_polypropylene.asp>.

[7] Dupont, "Summary of Properties for Kapton Polyimide Films," November 5, 2012. <http://www2.dupont.com/Kapton/en_US/assets/downloads/pdf/summaryofprop.pdf>.

[8] K-Mac Plastics, "Ultem 1000 Technical Property Data," November 28, 2012. <http://k-mac-plastics.net/data%20sheets/ultem_1000_technical_property_data.htm>.

[9] Southward, Robin; Thompson, D.W.;"Inverse Chemical Vapor Deposition: A Novel Single Stage Synthesis of Highly Reflective and Conductive Silvered Polymeric Films," *Chem. Mater.*, **11**, 501-507 (1999).

[10] Warner, J.; Pevzner, M.; Dean, C.J.; Kranbuehl, D.E.; Scott, J.L.; Broadwater, S.T.; Thompson, D.W.; Southward, R. "Synthesis of hexafluoroisopropylidene-containing polyimide-silver nanocomposite films evolving specularly reflective metal surfaces," *J. Mater. Chem.*, **13**, 1847-1852 (2003).

[11] Thompson, S.; Davis, L.; Thompson, D.; Southward, Robin. "Single-Stage Synthesis and Characterization of Reflective and Conductive Silver-Polyimide Films Prepared from Silver (1) Complexes with ODPA/4,4'-ODA," *ACS Applied Materials and Interfaces*, **1(7)**, 1457-1466 (2009).

[12] International Scientific Inc. "Polyimide Nanocomposite Circuit Board Materials to Mitigate Internal Electrostatic Discharge," NASA Phase I STTR Final Report, NNX11CI31P.

[13] Hu, L.Y.; Yang, S.; Miller, A.K.; Park, C.S.; Plichta, K.A.; Rochford, S.; Schulz, M.E.; Orwoll, R.A.; Jensen, B.J., "Aliphatic/Aromatic Hybrid Polymers for Functionally Graded Radiation Shielding," *High Performance Polymers*, **18**, 213-25 (2006).

[14]Cucinotta, Francis, "Radiation Risk Acceptability and Limitations."

[15] "The 2007 Recommendations of the International Commission on Radiological Protection". *Annals of the ICRP* publication 103 37 (2-4), (2007). November 7, 2012. <http://www.icrp.org/docs/ICRP_Publication_103-Annals_of_the_ICRP_37%282-4%29-Free_extract.pdf>.

[16] Kim, M.Y.; Thibeault, S.A.; Wilson, J.W.; Kiefer, R.L.; Orwoll, R.A. (1994). "Performance of Polymeric Materials as Shielding for Cosmic Radiation," *Irradiation of Polymers: Fundamentals and Technological Applications,* ACS Symposium Series 620 (1996).

[17] Smid, J.; Cabasso, I.; Obligin, A.; Rawls, H.R., US Patent. "Novel Radiopaque Heavy Metal Polymer Complexes, Compositions of Matter and Articles Prepared Therefrom," (1989).

[18] NASA Jet Propulsion Laboratory.

[19] Thibeault, S.A., Cooke, S.A., Ashe, M.P., Saucillo, R.J., Murphy, D.G., de Groh, K.K., Jaworske, D.A., Nguyen, Q.V., "MISSE-X: An ISS External Platform for Space Environment Studies in the Post-Shuttle Era," IEEEAC paper #1708, Version 2, October 2010.